J. Fluid Mech. (1986), *vol.* 164, *pp.* 185–215
Printed in Great Britain

Taylor dispersion in concentrated suspensions of rotating cylinders

By A. NADIM, R. G. COX† AND H. BRENNER

Department of Chemical Engineering, Massachusetts Institute of Technology, Cambridge, MA 02139

(Received 24 January 1985 and in revised form 25 June 1985)

Laminar heat- or mass-transfer processes are theoretically investigated for two-dimensional spatially periodic suspensions of circular cylinders, each member of which rotates steadily about its own axis under the influence of an external couple. The novelty of the ensuing convective-diffusion phenomena derives from the absence of convective motion at the suspension lengthscale (the 'macroscale'), despite its presence at the interstitial or particle lengthscale (the 'microscale'). The latter fluid motion consists of a cellular vortex-like flow characterized by closed streamlines. These periodically closed streamlines give rise to a situation in which there exists no *net* flow at the macroscale. The resulting macroscale transport of heat or mass thus proceeds purely by conduction, the rate being characterized by a tensor diffusivity – dependent upon the angular velocity of the cylinders. Matched-asymptotic-expansion methods together with generalized Taylor dispersion theory are used to calculate this macroscale conductivity in the dual limit of large rotary Péclet numbers and small gap widths between adjacent cylinders. This prototype study illustrates the fact that the usual separation of transport processes into distinct convective and conductive contributions is not generally a scale-invariant concept; that is, microscale convectional contributions to the transport of heat or mass are not generally representable by corresponding macroscale convectional contributions to the transport. Possible applications of the analysis exist in the area of enhanced conduction rates in ferrofluids or other dipolar fluids rotating relative to a fixed external field (or conversely).

1. Introduction

An earlier (Brenner 1984), purely fluid-mechanical study of the rotation about their own axes of the individual particles in an otherwise quiescent laminar suspension revealed the existence of a suspension-scale antisymmetric stress tensor arising from the body couples required to sustain the steady rotation. The novelty of that calculation lay in the fact that momentum could be transported despite the suspension being macroscopically at rest. The present paper represents a companion study of the transport of heat in such apparently quiescent suspensions. The prototype example studied herein shows that the macroscopic transport process is purely conductive – as certainly would be expected of a system at rest – but possesses an effective conductivity that is functionally dependent upon the angular velocity Ω of the suspended particles about their own axes relative to the suspension as a whole.

† Permanent address: Department of Civil Engineering and Applied Mechanics, McGill University, Montreal, P.Q., Canada H3A 2K6.

This phenomenon violates the so-called 'principle of material frame indifference' (Truesdell & Toupin 1960), as was already shown to occur for its momentum-transport counterpart (Brenner 1984). The apparent violation is rationalized by the fact that, whereas the macroscale motion of the continuum is everywhere zero, the same is not true of the microscale motion. As a consequence, the usual subdivision of transport processes into convective and conductive contributions cannot be regarded as a scale-invariant concept. Rather, microscale convection and conduction here coalesce into a single, purely conductive transport mechanism at the macroscale. The latter process is governed by a suspension-scale form of Fourier's law, but with an angular velocity-dependent effective conductivity. Thus, in contrast with conventional, forced-convection heat-transfer processes, the convective contribution to the transport rate is here implicit rather than explicit in the analysis. We coin the term 'micro-convection' to describe this phenomenon. Equivalently, 'macroconvection' is absent.

Fusion of separate microscale convection and conduction processes into a single macroscale conduction- or dispersion-like process is characteristic of Taylor-dispersion phenomena (Taylor 1953; Aris 1956). Indeed, generalized (Brenner 1980*a*, *b*, 1982; Brenner & Adler 1982) Taylor-dispersion theory will be employed to bring the problem solution to fruition.

Kinematically, our prototype example involves the two-dimensional, spatially periodic, vortex-like flow engendered by a square array of almost-touching parallel circular cylinders, each rotating steadily about its symmetry axis in a Newtonian fluid under the action of an external couple exerted upon it from outside of the system. This spatially periodic suspension geometry permits highly concentrated systems to be analysed in a *rigorous* manner; furthermore, the 'almost-touching' lubrication limit enormously simplifies the requisite fluid-mechanical and concomitant convective-diffusive Taylor-dispersion (Brenner 1980*b*; Brenner & Adler 1982) calculations. For the case of a square array these equations are solved analytically for various parametric combinations of rotary Péclet number $Pe \gg 1$, non-dimensional gap width $\epsilon \ll 1$, and solid–fluid conductivity ratio κ. Numerical values of the effective dispersivity dyadic are provided for the dual cases $Pe\,\epsilon^2 \gg 1$ and $Pe\,\epsilon^2 = O(1)$. These reveal that the dispersivity in the plane of flow grows like $Pe^{\frac{1}{2}}$, whence this effective conductivity can be made arbitrarily large by increasing the particle rotation rate. Large transport rates thus become realizable in practice despite the absence of any suspension-scale motion.

2. Flow between rotating cylinders

Figure 1 represents a longitudinal view of a unit cell characterizing the indefinitely extended, two-dimensional, spatially periodic suspension. The identical circular cylinders (radii R), assumed to be of infinite length with longitudinal axes directed normal to the plane of the paper, are arranged with their centres fixed at adjacent points of a square lattice; δ is half the minimum gap between adjacent cylinders, whereas Ω is the magnitude of the angular velocity of each cylinder relative to the fixed lattice. Interstitial fluid surrounding the cylinders is assumed to be incompressible (density ρ) and Newtonian (viscosity μ). The velocity in the fluid then satisfies the Navier–Stokes and continuity equations together with the zero-normal-velocity and no-slip boundary conditions on the cylinder surfaces. In addition, in order to ensure no net fluid motion we require that there be no flux of fluid through the gaps between the cylinders.

In the limit $\epsilon \equiv \delta/R \to 0$, lubrication theory (Batchelor 1967) provides an asym-

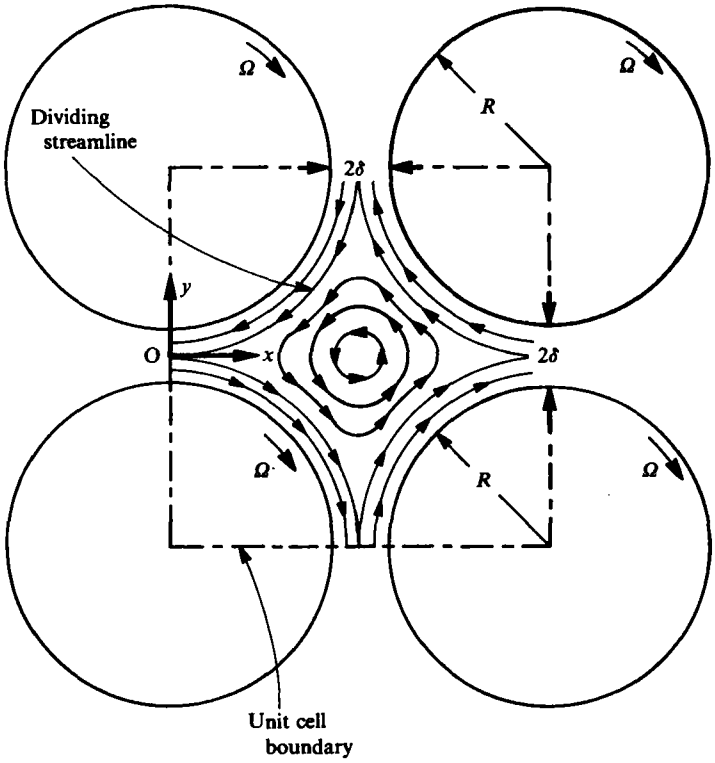

FIGURE 1. Longitudinal view of a four-cylinder unit cell of the square array.

ptotic approximation of the local flow field in the gap region. This will be found and matched onto an 'outer solution', valid in the fluid away from the gaps. As in figure 1, choose a rectangular Cartesian coordinate system (x, y) with the velocity components (u, v). Upon rendering distances dimensionless with R and velocities with $R\Omega$ the proper asymptotic scaling is

$$(\bar{x}, \bar{y}) = (\epsilon^{-\frac{1}{2}}x, \epsilon^{-1}y), \tag{2.1}$$

while it may be seen that (u, v) must be expanded as

$$u = \bar{u} + O(\epsilon), \quad v = \epsilon^{\frac{1}{2}}[\bar{v} + O(\epsilon)], \tag{2.2}$$

such that barred quantities are of order unity in the gap. In terms of the scaled coordinates $\bar{x}, \bar{y}$, each cylinder surface is described by

$$\bar{y} = \pm[1 + \tfrac{1}{2}\bar{x}^2 + O(\epsilon)]. \tag{2.3}$$

Provided that $Re\,\epsilon^{\frac{3}{2}} \ll 1$ (with $Re = R^2\Omega\rho/\mu$ the Reynolds number), the non-dimensional Navier–Stokes and continuity equations become, to terms of the lowest order in ϵ,

$$\frac{\partial^2 \bar{u}}{\partial \bar{y}^2} = \frac{\partial \bar{p}}{\partial \bar{x}}, \tag{2.4}$$

$$\frac{\partial \bar{p}}{\partial \bar{y}} = 0 \tag{2.5}$$

and

$$\frac{\partial \bar{u}}{\partial \bar{x}} + \frac{\partial \bar{v}}{\partial \bar{y}} = 0, \tag{2.6}$$

with $\bar{p} = \epsilon^{\frac{3}{2}} p/\mu\Omega$ the scaled pressure. These are to be solved subject to no-slip boundary conditions on the cylinder surfaces, which here take the forms

$$(\bar{u}, \bar{v}) = (-1, -\bar{x}) \quad \text{on } \bar{y} = 1 + \tfrac{1}{2}\bar{x}^2, \tag{2.7}$$

$$(\bar{u}, \bar{v}) = (1, -\bar{x}) \quad \text{on } \bar{y} = -(1 + \tfrac{1}{2}\bar{x}^2). \tag{2.8}$$

The zero-net-flow symmetry condition

$$\int_{-(1+\frac{1}{2}\bar{x}^2)}^{1+\frac{1}{2}\bar{x}^2} \bar{u}\, \mathrm{d}\bar{y} = 0 \tag{2.9}$$

through the gap must also be imposed.

These equations possess the solution

$$\bar{u} = -\bar{y}(1 + \tfrac{1}{2}\bar{x}^2)^{-1}, \tag{2.10}$$

$$\bar{v} = -\tfrac{1}{2}\bar{x}[1 + \bar{y}^2(1 + \tfrac{1}{2}\bar{x}^2)^{-2}]. \tag{2.11}$$

Equivalently, the stream function $\bar{\psi}$ is

$$\bar{\psi} = -\tfrac{1}{4}\bar{x}^2 + \bar{y}^2(2 + \bar{x}^2)^{-1} \tag{2.12}$$

to within an arbitrary additive constant. Here, $\bar{u} = -\partial\bar{\psi}/\partial\bar{y}$ and $\bar{v} = \partial\bar{\psi}/\partial\bar{x}$, so that by (2.2), if the unscaled velocity is written as $u = -\partial\psi/\partial y$ and $v = \partial\psi/\partial x$, we see that

$$\psi = \bar{\psi} + O(\epsilon).$$

As in figure 1, the streamline passing through the origin O is seen to be a dividing streamline. Though the solution (2.10)–(2.12) is valid only within the gap region, it nevertheless reveals the dominant features of the global flow field. In the gap itself the fluid motion is a 'saddle' flow, with fluid above the origin moving to the left and that below to the right. In the regions bounded between each cylinder surface and the dividing streamline the fluid particles traverse closed trajectories. Similarly in the midregion, symmetrically surrounded by the dividing streamlines of the four cylinders, a closed-streamline flow must necessarily exist – corresponding to a 'vortex' rotating in a direction opposite to that of the cylinders themselves.

The dividing streamline itself is described by $\bar{\psi} = 0$, whence

$$\bar{y} = \pm 2^{-\frac{1}{2}}\bar{x}(1 + \tfrac{1}{2}\bar{x}^2)^{\frac{1}{2}} \tag{2.13}$$

along this streamline. The two limiting domains

$$\bar{x} \to 0, \quad \bar{y} \sim \pm(2^{-\frac{1}{2}}\bar{x} + \ldots) \tag{2.14}$$

and

$$|\bar{x}| \to \infty, \quad \bar{y} \sim \pm(\tfrac{1}{2}\bar{x} + \tfrac{1}{2} + \ldots) \tag{2.15}$$

prove important in later discussion. In particular, comparison of (2.15) with (2.3) shows that as one moves out of the gap the distance of the dividing streamline from the cylinder surface approaches (in the scaled coordinates) a value of $\frac{1}{2}$ (cf. figure 2). Also, (2.14) reveals that the slope with which the dividing streamline approaches the origin in the scaled coordinates is $\pm 2^{-\frac{1}{2}}$.

In the gap, instead of using the scaled Cartesian coordinates $(\bar{x}, \bar{y})$, we can use new scaled coordinates $(\bar{\rho}, \bar{\theta})$ defined in terms of the polar coordinates (r, θ) shown in figure 3 as

$$\bar{\rho} = \frac{r-1}{\epsilon}, \quad \bar{\theta} = \frac{\frac{1}{2}\pi - \theta}{\epsilon^{\frac{1}{2}}}.$$

Since

$$x = +\cos\theta, \quad y = (1+\epsilon) - r\sin\theta,$$

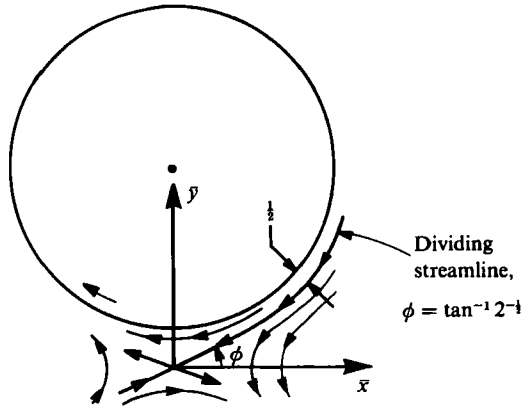

FIGURE 2. Dividing streamlines.

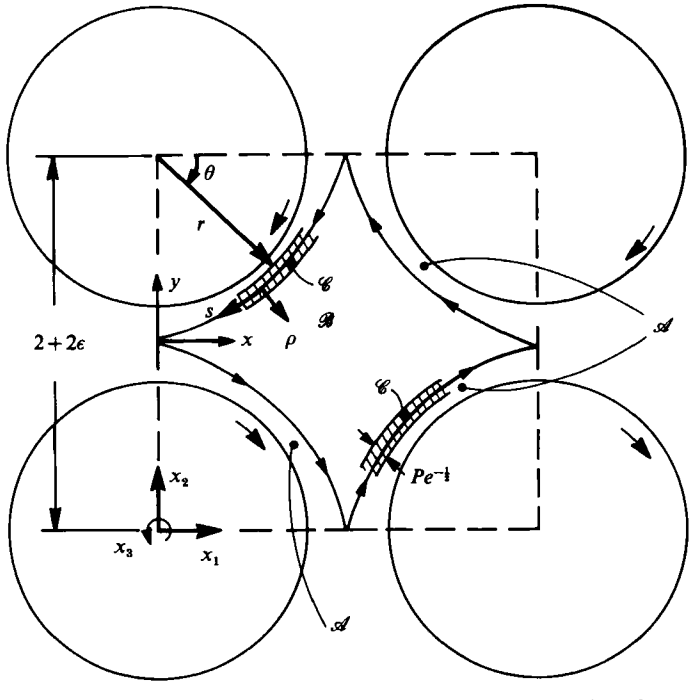

FIGURE 3. Two-dimensional Cartesian (x_1, x_2), circular cylindrical (r, θ), and intrinsic streamline (ρ, s) coordinates. Regions $\mathscr{A}, \mathscr{B}, \mathscr{C}$.

we can, by using (2.1), express $(\bar{x}, \bar{y})$ in terms of $(\bar{\rho}, \bar{\theta})$ as

$$\bar{x} = (\epsilon^{-\frac{1}{2}} + \epsilon^{\frac{1}{2}}\bar{\rho}) \sin(\epsilon^{\frac{1}{2}}\bar{\theta}),$$

$$\bar{y} = (\epsilon^{-1} + 1) - (\epsilon^{-1} + \bar{\rho}) \cos(\epsilon^{\frac{1}{2}}\bar{\theta}),$$

or, for $\epsilon \to 0$, as

$$\bar{x} \sim \bar{\theta} + O(\epsilon),$$

$$\bar{y} \sim (1 - \bar{\rho} + \tfrac{1}{2}\bar{\theta}^2) + O(\epsilon).$$

Thus, in the gap, $\bar{\psi}$, given by (2.12), may be written as

$$\bar{\psi} = -\tfrac{1}{4}\bar{\theta}^2 + \frac{(1-\bar{\rho}+\frac{1}{2}\bar{\theta}^2)^2}{(2+\bar{\theta}^2)} + O(\epsilon). \tag{2.16}$$

On moving out of the gap as $\bar{\theta} \to +\infty$ (and $\bar{x} \to \infty$), $\bar{\psi}$ takes the form

$$\bar{\psi} \sim [(\tfrac{1}{2}-\bar{\rho}) + O(\bar{\theta}^{-2})] + O(\epsilon). \tag{2.17}$$

This inner lubrication-theory solution (2.16), valid in the gap, must be matched onto an 'outer' solution valid away from the gap. However, we shall not require the details of this 'outer' flow field *per se*, but only the flow close to the cylinder surface. We thus perform only a local analysis of the 'outer' solution near the cylinder surface $r = 1$, and demonstrate that this can be rigorously matched onto the 'inner' lubrication solution (2.16). In order to do this we use $(\bar{\rho}, \theta)$ as independent variables for this 'local outer' expansion. Since, on the cylinder surface $r = 1$, we require that

$$v_\theta = -\frac{\partial \psi}{\partial r} = +1, \quad v_r = \frac{1}{r}\frac{\partial \psi}{\partial \theta} = 0,$$

we obtain, by expanding $\psi(r, \theta)$ about $r = 1$,

$$\psi(r,\theta) = \psi(1,\theta) + (r-1)\frac{\partial \psi}{\partial r}(1,\theta) + O(r-1)^2 = a - (r-1) + O(r-1)^2,$$

where a is a constant. This value of ψ at this order represents a uniform flow locally, and is therefore automatically a solution of the Navier-Stokes equation. Thus, for the 'local outer' solution, we obtain

$$\bar{\psi} = b - \bar{\rho} + O(\epsilon), \tag{2.18}$$

where b is a constant. For matching onto the 'inner' lubrication solution we require that (2.18), when expressed in terms of $(\bar{\rho}, \bar{\theta})$, has the same value for $\epsilon \to 0$ as $\bar{\psi}$ given by (2.17). Thus

$$b = \tfrac{1}{2},$$

giving the 'local outer' solution as

$$\bar{\psi} = (\tfrac{1}{2} - \bar{\rho}) + O(\epsilon). \tag{2.19}$$

Consequently, the limiting streamline $\bar{\psi} = 0$ away from the gap is given by

$$\bar{\rho} = \tfrac{1}{2},$$

or, equivalently,

$$r = 1 + \tfrac{1}{2}\epsilon,$$

so that this limiting streamline is situated at a constant distance of $\frac{1}{2}\epsilon$ from the cylinder surface (see figure 2). Also, from (2.19), the velocity field away from the gap (but close to the cylinder surface) is

$$v_\theta = 1 + O(\epsilon^2), \quad v_r = O(\epsilon^2), \tag{2.20}$$

so that this describes the flow on and near the dividing streamline.

Behaviour of the velocity along the dividing streamline may be found by substitution of (2.13) into (2.10) and (2.11), yielding

$$\bar{u}(\bar{\psi} = 0) = \pm \bar{x}(2+\bar{x}^2)^{-\frac{1}{2}}, \tag{2.21}$$

$$\bar{v}(\bar{\psi} = 0) = -\bar{x}(1+\bar{x}^2)(2+\bar{x}^2)^{-1}. \tag{2.22}$$

Again, in the two limiting domains it is found that

$$(\bar{u}, \bar{v}) \sim (\mp 2^{-\frac{1}{2}}\bar{x}, -\tfrac{1}{2}\bar{x}) \quad \text{as } \bar{x} \to 0 \tag{2.23}$$

and

$$(\bar{u}, \bar{v}) \sim (\mp 1, -\bar{x}) \quad \text{as } |\bar{x}| \to \infty, \tag{2.24}$$

while outside the gap the velocity on the dividing streamline is given by

$$(v_r, v_\theta) \sim (0, 1),$$

so that it is the same as that at the cylinder surface. The details of the flow in the outer region away from the cylinder walls will not be required. However it is to be noted that it may be shown (using symmetry and the fact that the creeping-flow equations are linear) that beyond the dividing streamline (away from the cylinders) all streamlines are closed, whence that the general flow pattern is expected to be like that shown in figure 1.

Summarizing our kinematical conclusions, closed streamlines exist adjacent to the cylinders as well as in the midregion away from the cylinders. Outside the gap region the streamline separating these domains lies at a dimensionless distance $\frac{1}{2}\epsilon$ from each cylinder surface, with the dimensionless velocity being unity (at lowest order) on that streamline.

3. Dispersion in periodic suspensions

The assumed spatial periodicity of the velocity field renders the current problem soluble by generalized Taylor dispersion methods (Brenner 1980*b*; Brenner & Adler 1982) applied to such systems. Within that framework, application of a moment analysis to the microscale convective-diffusion equations governing transport of a tracer particle in a spatially periodic medium leads to the conclusion that the macroscale tracer transport can itself generally be described by a convective-diffusion equation (with position- and time-independent phenomenological coefficients), asymptotically valid for long times. Thus, provided that the times of interest greatly exceed the microscale (i.e. unit-cell) diffusive 'equilibration' time, the theory provides expressions for the mean velocity and Taylor dispersivity describing the macroscale transport.

In applying existing dispersion theory (Brenner 1980*b*; Brenner & Adler 1982), we consider the elementary case of a pointsize, neutrally buoyant tracer particle characterized by a partition coefficient of unity – the latter describing the equilibrium tracer distribution amongst the fluid and solid phases of the suspension. Such circumstances equally well describe heat transfer. As such, the Taylor dispersivity dyadic eventually obtained in a mass-transfer context is applicable to more general types of transport processes.

In present circumstances it is readily proved (Brenner 1984) that the macroscale velocity is zero. Explicitly,

$$\overline{\boldsymbol{U}}^* = \boldsymbol{0}. \tag{3.1}$$

This is an immediate consequence of two facts: (i) the zero-net-fluid-flow condition (2.9) existing across the boundaries of each unit cell of the suspension, which gives rise to the zero volume-average condition†

$$\int_{\mathcal{V}} \boldsymbol{v}\, \mathrm{d}\boldsymbol{r} = \boldsymbol{0} \tag{3.2}$$

† In the interests of clarity the reader should note that dimensional quantities are used in (3.2)–(4.4), whereas in § 2 and in (4.5), as well as in most subsequent equations, non-dimensional quantities are used. Exceptions to the latter rule will be obvious.

within the *fluid* region $\boldsymbol{r} \in \boldsymbol{r}_f$; (ii) a zero-net-*solid*-phase-velocity condition arising from the fact that each cylinder rotates about a fixed point, and hence necessarily possesses zero volume-average translational velocity, i.e.

$$\int_{r_s} \boldsymbol{\Omega} \times \boldsymbol{r} \, d\boldsymbol{r} = \boldsymbol{0} \tag{3.3}$$

within the cylinder interiors $\boldsymbol{r} \in \boldsymbol{r}_s$.

Since (3.1) shows macroconvention to be absent, macroscale transport necessarily occurs exclusively by macroconduction; however, microconvection will be seen to play a dominant role in determining the effective conductivity of the suspension, at least at the large Péclet numbers subsequently considered.

The generic expression (Brenner & Adler 1982) for the suspension-scale Taylor-dispersivity dyadic here reduces to the form

$$\bar{\boldsymbol{D}}^* = \frac{1}{\tau_0}\left[D\int_{r_f} (\nabla \boldsymbol{B})^\dagger \cdot (\nabla \boldsymbol{B})\, d\boldsymbol{r} + D^s \int_{r_s} (\nabla \boldsymbol{B})^\dagger \cdot (\nabla \boldsymbol{B})\, d\boldsymbol{r}\right]. \tag{3.4}$$

The vector microfield $\boldsymbol{B}$ at point $\boldsymbol{r}$ satisfies the steady-state vector convective-diffusion equations

$$\boldsymbol{v} \cdot \nabla \boldsymbol{B} = D \nabla^2 \boldsymbol{B} \quad (\boldsymbol{r} \in \boldsymbol{r}_f), \tag{3.5}$$

$$\boldsymbol{v}^s \cdot \nabla \boldsymbol{B} = D^s \nabla^2 \boldsymbol{B} \quad (\boldsymbol{r} \in \boldsymbol{r}_s), \tag{3.6}$$

with $\boldsymbol{v}^s = \boldsymbol{\Omega} \times \boldsymbol{r}$ the solid velocity, together with the cylinder surface boundary conditions

$$\boldsymbol{B} \text{ continuous across } S_p, \tag{3.7}$$

$$D\boldsymbol{n} \cdot \nabla \boldsymbol{B}|_{\text{fluid}} = D^s \boldsymbol{n} \cdot \nabla \boldsymbol{B}|_{\text{solid}} \quad \text{on } S_p, \tag{3.8}$$

and unit-cell surface boundary conditions

$$[\![\boldsymbol{B}]\!] = -[\![\boldsymbol{r}]\!], \tag{3.9}$$

$$[\![\nabla \boldsymbol{B}]\!] = \boldsymbol{0}. \tag{3.10}$$

In this formulation the $\boldsymbol{B}(\boldsymbol{r})$ field is defined at all points $\boldsymbol{r} \in \boldsymbol{r}_0$ ($\boldsymbol{r}_0 = \boldsymbol{r}_f \oplus \boldsymbol{r}_s$) within a unit cell. The unit cell, whose volume is τ_0, consists of solid (s) and fluid (f) domains $\boldsymbol{r}_s$ and $\boldsymbol{r}_f$, possessing respective scalar diffusivities D^s and D to tracer transport. Further, S_p denotes the surface of the cylinders with $\boldsymbol{n}$ the unit outward-drawn normal. Appearing in (3.9) and (3.10) is the double-bracketed operator $[\![\ ]\!]$, which denotes the 'jump' in the value of its argument between geometrically equivalent points lying on opposite unit-cell faces.

The solution of equations (3.5)–(3.10) is unique only to within an arbitrary additive vector constant (Brenner & Adler 1982). This is of no physical import as (3.4) only involves derivatives of $\boldsymbol{B}$. Furthermore, if the solid phase is non-conducting ($D^s = 0$) the proper normalization for (3.4) is no longer $1/\tau_0$ but rather $1/\tau_f$. Correspondingly, in such circumstances the microscale 'equilibration' time – assumed small compared with times of interest – is then the characteristic time for the tracer to sample only the fluid points $\boldsymbol{r} \in \boldsymbol{r}_f$; formerly it was the time required to sample all the points, $\boldsymbol{r} \in \boldsymbol{r}_0$.

Subsequent portions of this paper are concerned with the actual computation of $\bar{\boldsymbol{D}}^*$ in several circumstances of interest. The first of these corresponds to the limiting case where the solid phase is impermeable to tracer transport (non-conducting cylinders).

4. Transport within the fluid phase only

For the degenerate case $D^s = 0$ the $\boldsymbol{B}$ field is only defined within the fluid-containing region $\boldsymbol{r} \in \boldsymbol{r}_f$ of the unit cell. Therein it satisfies the steady-state convective-diffusion equation

$$\boldsymbol{v}\cdot\nabla\boldsymbol{B} = D\nabla^2\boldsymbol{B}, \tag{4.1}$$

together with the particle and cell boundary conditions

$$\boldsymbol{n}\cdot\nabla\boldsymbol{B} = \boldsymbol{0} \quad \text{on } S_p, \tag{4.2}$$

$$[\![\boldsymbol{B}]\!] = -[\![\boldsymbol{r}]\!], \tag{4.3}$$

$$[\![\nabla\boldsymbol{B}]\!] = \boldsymbol{0}. \tag{4.4}$$

Write $\boldsymbol{B} = B_1\boldsymbol{i}_1 + B_2\boldsymbol{i}_2 + B_3\boldsymbol{i}_3$ with $(\boldsymbol{i}_1, \boldsymbol{i}_2, \boldsymbol{i}_3)$ unit vectors along the right-handed Cartesian coordinates depicted in figure 3. This permits independent equations to be set forth separately for each component B_i of $\boldsymbol{B}$. Specifically the transport equation governing $B = B_2/R$ may be written in the non-dimensional form

$$\boldsymbol{v}\cdot\nabla B = Pe^{-1}\nabla^2 B, \tag{4.5}$$

subject to

$$\boldsymbol{n}\cdot\nabla B = 0 \quad \text{on } S_p, \tag{4.6}$$

$$[\![B]\!]_j = \begin{cases} -2(1+\epsilon) & (j=2), \\ 0 & (j=1,3), \end{cases} \tag{4.7, 4.8}$$

and

$$[\![\nabla B]\!]_j = \boldsymbol{0} \quad (j=1,2,3), \tag{4.9}$$

with $Pe = R^2\Omega/D$ the rotary Péclet number. Here, for example,

$$[\![B]\!]_2 = B(x_1, 2(1+\epsilon), x_3) - B(x_1, 0, x_3).$$

For $Pe \gg 1$ the characteristic convective tracer transport time is much less than that for molecular diffusion. It is apparent in this limit that, away from (boundary-layer) regions where second derivatives are important, (4.5) reduces to

$$\boldsymbol{v}\cdot\nabla B = 0 \tag{4.10}$$

to terms of lowest order. The latter implies that B is constant along streamlines, whence B is necessarily of the intrinsic form $B = f(\psi)$ with ψ the two-dimensional stream function. In regions of closed streamlines it can further be shown that the diffusion term in (4.5) has the effect of rendering B independent of the coordinate transverse to the streamlines. Together with (4.10) this leads to the conclusion that B is necessarily constant in the entire closed-streamline region. The proof entails showing that $f'(\psi) = 0$ in such regions.

To this end choose an arbitrary closed streamline ψ = constant, which may either completely enclose fluid or surround a cylinder. Integrate (4.5) over the entire fluid area $A(\psi)$ interior to that streamline to obtain

$$\int_{A(\psi)} \nabla\cdot[\boldsymbol{v}B - Pe^{-1}\nabla B]\,\mathrm{d}A = -Pe^{-1}\oint_{C(\psi)} \boldsymbol{v}\cdot\nabla B\,\mathrm{d}l = 0. \tag{4.11}$$

Use has been made of the divergence theorem in conjunction with boundary condition (4.6); $\boldsymbol{v}$ is the outward normal to the closed streamline, while curve $C(\psi)$ denotes the closed streamline. Introduce $B = f(\psi)$ into (4.11) to obtain

$$f'(\psi)\oint_{C(\psi)} \boldsymbol{v}\cdot\nabla\psi\,\mathrm{d}l = 0. \tag{4.12}$$

Since, by definition, $\boldsymbol{v} = \nabla\psi/|\nabla\psi|$ (or the negative thereof), the above integrand is non-zero and of the same algebraic sign along the entire integration contour. Thus

$$f'(\psi) = 0, \tag{4.13}$$

as was to be demonstrated. This equation necessarily obtains throughout the entire closed-streamline region, since the particular streamline chosen for its proof was arbitrary. Equations (4.10) and (4.13) imply that B is constant along and across the streamlines; B is therefore necessarily constant within the closed-streamline domains of the flow. This conclusion is not novel; other contexts (Acrivos 1971; Frankel & Acrivos 1968; Cox, Zia & Mason 1968; Torza *et al.* 1971; Rhines & Young 1983) involving the steady-state convective-diffusion transport of passive scalars in regions of closed streamlines lead to the same condition.

In the present circumstances the flow pattern consists entirely of closed-streamline regions separated by dividing streamlines. Jump condition (4.7), however, precludes the possibility that B possesses the same constant value throughout the whole domain $\boldsymbol{r} \in \boldsymbol{r}_f$. Rather, in a later section it will be demonstrated that B attains a different constant value in the central vortex region than in the closed-streamline regions adjacent to the cylinders. Hence, large gradients in B must obtain in the vicinity of the dividing streamline, in which region neglect of the right-hand side of (4.5) is no longer justified. It therefore becomes necessary to derive 'inner' equations, valid in the boundary layers straddling the dividing streamlines. As $\bar{\boldsymbol{D}}^*$ depends upon gradients of $\boldsymbol{B}$ [cf. (3.4)] it is to be expected that the major contribution to $\bar{\boldsymbol{D}}^*$ arises from such boundary layers. This warrants a detailed inner-field analysis, which is performed in the next section.

5. Inner analysis

Equation (4.5) may be written in the cylindrical polar coordinate system shown in figure 3 as

$$\frac{1}{r}\frac{\partial}{\partial r}\left(r\frac{\partial B}{\partial r}\right)+\frac{1}{r^2}\frac{\partial^2 B}{\partial\theta^2} = Pe\left[\frac{1}{r}\frac{\partial}{\partial r}(rv_r B)+\frac{1}{r}\frac{\partial}{\partial\theta}(v_\theta B)\right]. \tag{5.1}$$

In these coordinates, and away from the gap, the dividing streamline is located at $r = 1+\frac{1}{2}\epsilon$. In order to retain the diffusion terms in the boundary layer straddling the dividing streamline, we therefore define scaled streamline coordinates (ρ, s) by the relations

$$r = 1+\tfrac{1}{2}\epsilon+Pe^{-\frac{1}{2}}\rho, \tag{5.2}$$

$$s = r\theta. \tag{5.3}$$

Substitution into (5.1) in conjunction with the facts that $v_\theta \sim 1$ and $v_r \sim 0$ outside the gap thereby yields

$$\frac{\partial^2 B}{\partial\rho^2} = \frac{\partial B}{\partial s} \tag{5.4}$$

to terms of lowest order in ϵ and $Pe^{-\frac{1}{2}}$. Within the boundary-layer region of thickness $O(Pe^{-\frac{1}{2}})$ straddling the dividing streamline, transverse diffusion is therefore balanced by convection along the dividing streamline. It will further be supposed that $Pe^{-\frac{1}{2}} \ll \epsilon$, whence the boundary layer remains well away from the cylinder surfaces.

Recapitulating, the prior analysis reveals that, in the limiting case

$$Pe\,\epsilon^2 \gg 1, \tag{5.5}$$

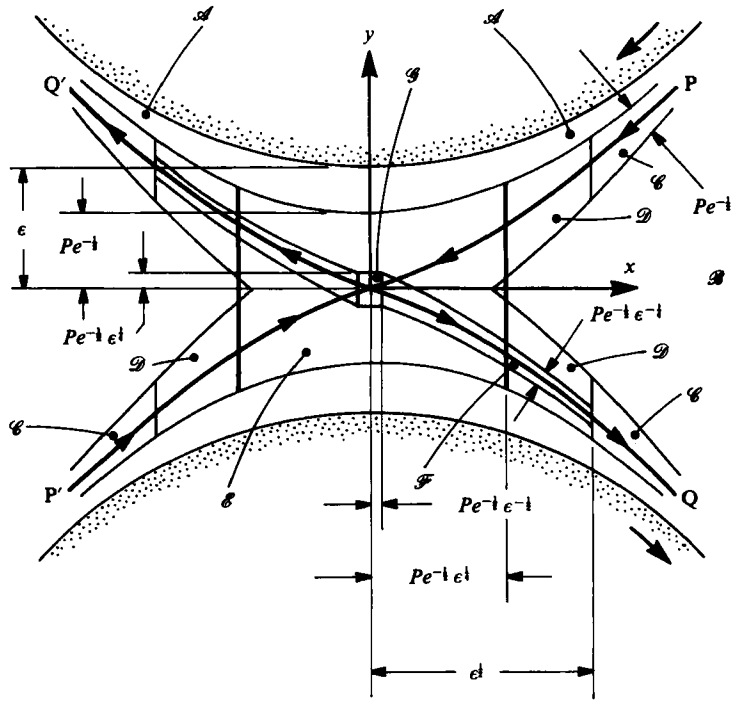

FIGURE 4. Gap regions.

(5.4) obtains in region $\mathscr{C}$ (figure 3) separating areas $\mathscr{A}$, adjacent to the cylinders, from region $\mathscr{B}$, the vortex region. In both of these regions B possesses constant, position-independent values. However, (5.4) has been derived only for the domain away from the gap; within the gap the possible existence of other convective-diffusive regimes must be recognized.

Specifically, referring to figure 4 and recalling that the dividing streamline approaches the origin with a slope of order $\frac{1}{2}\epsilon^{\frac{1}{2}}$ (figure 2), it is found that the boundary layers $\mathscr{C}$ of two adjacent cylinders merge at a distance of order $Pe^{-\frac{1}{2}}\epsilon^{-\frac{1}{2}}$ from the origin centred in the gap. Within that region (labelled $\mathscr{E}$) the proper scaling for the gap coordinates is thus

$$(\hat{x}, \hat{y}) = (Pe^{\frac{1}{2}}\epsilon^{\frac{1}{2}}x,\ Pe^{\frac{1}{2}}y). \tag{5.6}$$

In conjunction with (2.1), (2.2), (2.10) and (2.11) this provides the pertinent velocity normalizations

$$(\hat{u}, \hat{v}) = (Pe^{\frac{1}{2}}\epsilon u,\ Pe^{\frac{1}{2}}\epsilon^{\frac{1}{2}}v) \sim (-\hat{y}, -\tfrac{1}{2}\hat{x}). \tag{5.7}$$

The (x, y)-space convective-diffusion equation

$$\left(\frac{\partial^2}{\partial x^2}+\frac{\partial^2}{\partial y^2}\right)B = Pe\left(u\frac{\partial B}{\partial x}+v\frac{\partial B}{\partial y}\right) \tag{5.8}$$

governing the B-field thereby adopts the form

$$\hat{y}\frac{\partial B}{\partial \hat{x}}+\tfrac{1}{2}\hat{x}\frac{\partial B}{\partial \hat{y}} = 0 \quad \text{in } \mathscr{E} \tag{5.9}$$

to terms of lowest order in the parameters $Pe^{-\frac{1}{2}}$, $\epsilon^{\frac{1}{2}}$ and $\epsilon^{-2}Pe^{-1}$. This equation reveals convection to be the dominant mode by which B is transported in region $\mathscr{E}$. This

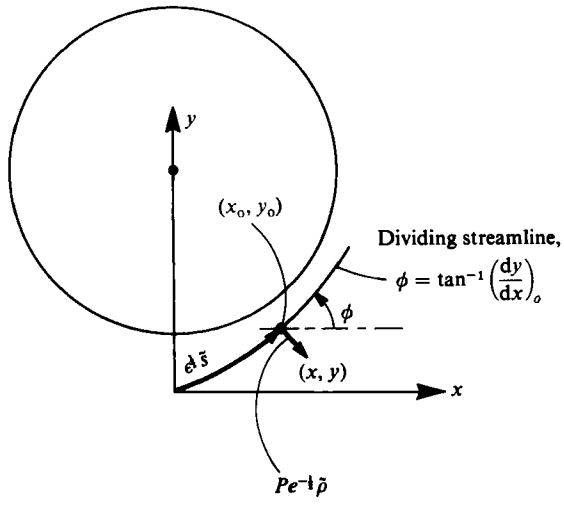

FIGURE 5. Intrinsic streamline coordinates $(\tilde{s}, \tilde{\rho})$ in the gap region.

contrasts with the comparable conclusion [cf. (5.4)] reached for the boundary-layer region $\mathscr{C}$.

The domain labelled $\mathscr{D}$ in figure 4 provides a transition region between $\mathscr{C}$ and $\mathscr{E}$. Here, the x-coordinate is $O(\epsilon^{\frac{1}{2}})$, as too is the length of the gap region [cf. (2.1)]. However, in order to find the properly scaled equation for B we must consider scaled coordinates along $(\epsilon^{\frac{1}{2}}\tilde{s})$ and transverse $(Pe^{-\frac{1}{2}}\tilde{\rho})$ to the dividing streamline. Toward this end consider the coordinate system depicted in figure 5. Point (x, y) is given functionally in terms of $\tilde{\rho}$ and the corresponding point (x_0, y_0) on the dividing streamline by the pair of relations

$$x = x_0 + Pe^{-\frac{1}{2}}\tilde{\rho}\sin\phi = x_0 + Pe^{-\frac{1}{2}}\tilde{\rho}\left(\frac{\partial y}{\partial x}\right)_0\left[1+\left(\frac{\partial y}{\partial x}\right)_0^2\right]^{-\frac{1}{2}} \tag{5.10}$$

and

$$y = y_0 - Pe^{-\frac{1}{2}}\tilde{\rho}\cos\phi = y_0 - Pe^{-\frac{1}{2}}\tilde{\rho}\left[1+\left(\frac{\partial y}{\partial x}\right)_0^2\right]^{-\frac{1}{2}}. \tag{5.11}$$

Concurrently, point (x_0, y_0) is uniquely determined by specifying $\tilde{s}$ through the definitions

$$\epsilon^{\frac{1}{2}}\tilde{s} = \int_0^{x_0}\left[1+\left(\frac{\partial y}{\partial x}\right)^2\right]^{\frac{1}{2}} dx = \int_0^{y_0}\left[1+\left(\frac{\partial x}{\partial y}\right)^2\right] dy, \tag{5.12}$$

in which the integrands are to be evaluated on the dividing streamline. Make use of (2.13) in conjunction with (2.1) to evaluate $(\tilde{s}, \tilde{\rho})$ from the above in terms of $(\bar{x}, \bar{y})$. This yields

$$\tilde{s} \sim \bar{x}, \tag{5.13}$$

$$Pe^{-\frac{1}{2}}\epsilon^{-1}\tilde{\rho} \sim 2^{-\frac{1}{2}}\bar{x}(1+\tfrac{1}{2}\bar{x}^2)^{\frac{1}{2}} - \bar{y} \tag{5.14}$$

to terms of lowest order in ϵ.

Coordinates $(s, \rho) = (\epsilon^{\frac{1}{2}}\tilde{s}, Pe^{-\frac{1}{2}}\tilde{\rho})$ become rectilinear (Cartesian) in the dual limit $\epsilon \to 0$ and $Pe \to \infty$ as may be verified from (5.13) and (5.14). Consequently, the B-field equation (4.5) adopts the form

$$\frac{\partial^2 B}{\partial s^2} + \frac{\partial^2 B}{\partial \rho^2} = Pe\left(v_\rho \frac{\partial B}{\partial \rho} + v_s \frac{\partial B}{\partial s}\right), \tag{5.15}$$

correct to terms of dominant order. Intrinsic velocity components (v_ρ, v_s) appearing in (5.15) may be evaluated from (2.10) and (2.11) via the coordinate transformations

$$v_\rho(x,y) = u(x,y)\cos\phi + v(x,y)\sin\phi, \tag{5.16}$$

$$v_s(x,y) = u(x,y)\sin\phi - v(x,y)\cos\phi. \tag{5.17}$$

Angle ϕ is identical with that appearing in (5.10) and (5.11) (figure 5). Evaluation of the right-hand sides of (5.16) and (5.17) furnishes the proper normalizations of the respective velocity components. Explicitly,

$$(v_s, v_\rho) = (\tilde{v}_s,\ Pe^{-\frac{1}{2}}\epsilon^{-\frac{1}{2}}\tilde{v}_\rho), \tag{5.18}$$

wherein $\tilde{v}_s = -2^{-\frac{1}{2}}\tilde{s}(1+\frac{1}{2}\tilde{s}^2)^{-\frac{1}{2}}$ and $\tilde{v}_\rho = 2^{-\frac{1}{2}}(1+\frac{1}{2}\tilde{s}^2)^{-\frac{3}{2}}\tilde{\rho}$ are of order unity. Substitution into (5.15) yields at lowest order

$$-\tilde{s}(1+\tfrac{1}{2}\tilde{s}^2)\frac{\partial B}{\partial \tilde{s}} + \tilde{\rho}\frac{\partial B}{\partial \tilde{\rho}} = 0 \quad \text{in } \mathscr{D}, \tag{5.19}$$

governing the transport of B within the indicated region.

These observations demonstrate that in both gap regions $\mathscr{E}$ [cf. (5.9)] and $\mathscr{D}$ [cf. (5.19)] the dominant transport mechanism is convection, whence B is constant along the streamlines. As such, along the dividing streamline PP′ in figure 4 the value of B remains constant on each side of the origin. However, since the flows from both P and P′ converge at the origin, and since the value of B at P′ differs from that at P, large gradients in B necessarily obtain at the origin, as well as on the dividing streamline QQ′. Hence, the regions $\mathscr{F}$ and $\mathscr{G}$ shown in the figure require further elaboration.

In the areal domain $\mathscr{F}$ assign the symbol λ to the transverse coordinate scaling in (5.15). An order-of-magnitude balance of diffusion $\partial^2 B/\partial\rho^2$ in the transverse direction against convection $Pe\, v_s \partial B/\partial s$ along the dividing streamline, considered in conjunction with the orderings $v_s \sim O(1)$ and $s \sim O(\epsilon^{\frac{1}{2}})$, thereby yields $\lambda = Pe^{-\frac{1}{2}}\epsilon^{\frac{1}{4}}$. Hence, the sub-boundary-layer region $\mathscr{F}$ is of width $Pe^{-\frac{1}{2}}\epsilon^{\frac{1}{4}}$ extended along the dividing streamline QQ′ in the gap. Within $\mathscr{F}$, diffusion in the transverse direction is once again important. The equation governing transport in the latter domain may be derived as follows: Choose coordinates $s^* = \epsilon^{-\frac{1}{2}}s$ and $\rho^* = Pe^{\frac{1}{2}}\epsilon^{-\frac{1}{4}}\rho$ in accordance with the proper lengthscales in $\mathscr{F}$. Observe then that the velocity components scale according to

$$(v_s^*, v_\rho^*) = (v_s,\ Pe^{\frac{1}{2}}\epsilon^{\frac{1}{4}}v_\rho). \tag{5.20}$$

Substitute these results into (5.15) to eventually obtain

$$2^{-\frac{1}{2}}(1+\tfrac{1}{2}s^{*2})^{-\frac{3}{2}}\rho^*\frac{\partial B}{\partial \rho^*} - 2^{-\frac{1}{2}}s^*(1+\tfrac{1}{2}s^{*2})^{-1}\frac{\partial B}{\partial s^*} = \frac{\partial^2 B}{\partial \rho^{*2}} \quad \text{in } \mathscr{F}, \tag{5.21}$$

describing transport in this region at lowest order.

In the region $\mathscr{G}$ near to the origin the flow differs from that which obtains along the remainder of domain $\mathscr{F}$. Upon consideration of the slope of the dividing streamline near the origin, this saddle-flow region $\mathscr{G}$ can be shown to be of width $Pe^{-\frac{1}{2}}\epsilon^{-\frac{1}{4}}$ in the x-direction (as depicted in figure 4). If x^* and y^* are the coordinates used in this region, so that

$$(x^*, y^*) = (Pe^{\frac{1}{2}}\epsilon^{\frac{1}{4}}x,\ Pe^{\frac{1}{2}}\epsilon^{-\frac{1}{4}}y), \tag{5.22}$$

the corresponding velocity components may be shown to scale according to

$$(u^*, v^*) = (Pe^{\frac{1}{2}}\epsilon^{\frac{3}{4}}u,\ Pe^{\frac{1}{2}}\epsilon^{\frac{1}{4}}v). \tag{5.23}$$

Region	Number of regions within cell	Description	Diffusion important?	Area	$\lvert\nabla B\rvert$	$\lvert\nabla B\rvert^2 \times$ area
$\mathscr{A}$	4	B constant	—	1	$o(1)$	$o(1)$
$\mathscr{B}$	1	B constant	—	1	$o(1)$	$o(1)$
$\mathscr{C}$	4	Boundary layer; constant velocity	Yes	$Pe^{-\frac{1}{2}}$	$Pe^{\frac{1}{2}}$	$Pe^{\frac{1}{2}}$
$\mathscr{D}$	8	Boundary layer; variable velocity	No	$Pe^{-\frac{1}{2}}\epsilon^{\frac{1}{2}}$	$Pe^{\frac{1}{2}}$	$Pe^{\frac{1}{2}}\epsilon^{\frac{1}{2}}$
$\mathscr{E}$	4	Saddle-flow region	No	$Pe^{-1}\epsilon^{-\frac{1}{2}}$	$Pe^{\frac{1}{2}}$	$\epsilon^{-\frac{1}{2}}$
$\mathscr{F}$	4	Boundary layer: variable velocity	Yes	$Pe^{-\frac{1}{2}}\epsilon^{\frac{1}{2}}$	$Pe^{\frac{1}{2}}\epsilon^{-\frac{1}{4}}$	$Pe^{\frac{1}{2}}\epsilon^{\frac{1}{4}}$
$\mathscr{G}$	4	Saddle-flow 'point'	Yes	Pe^{-1}	$Pe^{\frac{1}{2}}\epsilon^{-\frac{1}{4}}$	$\epsilon^{-\frac{1}{2}}$

TABLE 1. Orders of magnitude of $\lvert\nabla B\rvert^2 \times$ area for the distinct flow regions

Substitution of these results in (5.8) yields the lowest-order form

$$-y^*\frac{\partial B}{\partial x^*}-\tfrac{1}{2}x^*\frac{\partial B}{\partial y^*}=\frac{\partial^2 B}{\partial y^{*2}} \quad \text{in } \mathscr{G}. \tag{5.24}$$

Actual dimensions of the various regions depicted in figure 4 have been exaggerated for pictorial clarity. This is evidenced by the existence of the inequalities

$$Pe^{-\frac{1}{2}}\epsilon^{\frac{1}{2}} \ll Pe^{-\frac{1}{2}} \ll \epsilon \ll \epsilon^{\frac{1}{2}} \tag{5.25}$$

and

$$Pe^{-\frac{1}{2}}\epsilon^{-\frac{1}{4}} \ll Pe^{-\frac{1}{2}}\epsilon^{-\frac{1}{2}} \ll \epsilon^{\frac{1}{2}} \tag{5.26}$$

in conjunction with inequality (5.5).

Prior to deriving the detailed solutions of the B equations for the various regions, it is instructive to consider an order-of-magnitude analysis of the respective contribution of each such region to the expression (3.4) for the Taylor dispersivity. In present circumstances the solution for B_2 yields the component

$$\overline{D}^*_{22}=\frac{D}{A_{\mathrm{f}}}\int_{A_{\mathrm{f}}}(\nabla B_2)\cdot(\nabla B_2)\,\mathrm{d}A \tag{5.27}$$

of the complete dispersivity dyadic, in which area A_{f} denotes the (two-dimensional) domain occupied by fluid within the unit cell. The length to be assigned to the unit cell along the x_3 direction (i.e. normal to the plane of the paper in figure 3) is without consequence since B_2 is independent of x_3.

Equation (5.27) may be written in the dimensionless form

$$\frac{\overline{D}^*_{22}}{D}=\frac{1}{A_{\mathrm{f}}}\int_{A_{\mathrm{f}}}(\nabla B)\cdot(\nabla B)\,\mathrm{d}A, \tag{5.28}$$

whose integrand is amenable to order-of-magnitude analysis. Table 1 tabulates the various regions composing the domain $\boldsymbol{r}\in\boldsymbol{r}_{\mathrm{f}}$, along with their respective contributions to the dispersivity (5.28). Scrutiny of the entries in the last column of that table, together with inequalities (5.25) and (5.26), leads to the conclusion that the dominant contribution to the dispersivity arises from regions $\mathscr{C}$. Consequently, the Taylor

dispersivity $\bar{D}^*_{22}$ will exhibit the functional dependence

$$\frac{\bar{D}^*_{22}}{D} \sim Pe^{\frac{1}{2}} \tag{5.29}$$

in the dual limits $Pe \gg 1$ and $\epsilon \ll 1$, with $Pe\,\epsilon^2 \gg 1$. Contributions arising from the other regions are obviously negligible in comparison with $Pe^{\frac{1}{2}}$.

As regions $\mathscr{C}$ (of which there are four in the unit cell) provide the major contributions to the dispersivity, it proves sufficient for purposes of the dispersivity calculation only to solve (5.4) for $B(s,\rho)$ in each of the boundary-layer regions $\mathscr{C}$ of the unit cell. Prerequisite to this solution is establishment of the proper boundary/matching conditions that need be imposed to determine B uniquely. Derivation of these necessitates certain symmetry arguments, discussed in the following section.

6. Boundary/matching conditions

Equations (4.5)–(4.9) governing the microfield B are invariant under the transformation $(B,\boldsymbol{r})\rightarrow(-B,-\boldsymbol{r})$, where $\boldsymbol{r}$ is the two-dimensional position vector measured from a centre of symmetry, such as O′ or O″ in figure 6. As such, it follows that $B(\mathrm{T}') - B(\mathrm{O}') = -B(\mathrm{W}') + B(\mathrm{O}')$. A relationship of the same form can be obtained for the corresponding doubly primed points if we correspondingly denote by $B(\mathrm{O}'')$ the constant value of B on the surface of the cylinder centered at O″. (Note that in the present circumstances B is not defined within the solid phase.) This leads to the pair of relations

$$B(\mathrm{T}') + B(\mathrm{W}') = 2B(\mathrm{O}'), \tag{6.1}$$

$$B(\mathrm{T}'') + B(\mathrm{W}'') = 2B(\mathrm{O}''), \tag{6.2}$$

for any generic pair of points (T′, W′) or (T″, W″) symmetrically disposed about O′ or O″.

In reference to figure 6, B was shown to attain constant values in each of regions $\mathscr{B}, \mathscr{A}_1, \mathscr{A}_2, \mathscr{A}_3, \mathscr{A}_4$. That B is determined only to within an arbitrary additive constant allows us to arbitrarily set $B(\mathscr{A}_1) = 0$. Jump conditions (4.7) and (4.8) then imply that

$$B(\mathscr{A}_1) = B(\mathscr{A}_2) = 0 \tag{6.3}$$

and

$$B(\mathscr{A}_3) = B(\mathscr{A}_4) = 2 \tag{6.4}$$

to terms of dominant order, whereas symmetry result (6.1) dictates that

$$B(\mathscr{B}) = 1. \tag{6.5}$$

On the dividing streamline PQRSP in figure 6, choose $s = 0$ at point P. In conjunction with definitions (5.2) and (5.3), points Q, R and S are respectively given by $s = \frac{1}{2}\pi$, π and $\frac{3}{2}\pi$ to dominant order. Hence, the governing transport equation for boundary-layer domain $\mathscr{C}$ becomes

$$\frac{\partial^2 B}{\partial \rho^2} = \frac{\partial B}{\partial s} \quad (0 \leqslant s \leqslant 2\pi,\ -\infty < \rho < \infty). \tag{6.6}$$

Since, by the symmetry result (6.1),

$$B(s+\pi,\rho) = 2 - B(s,\rho), \tag{6.7}$$

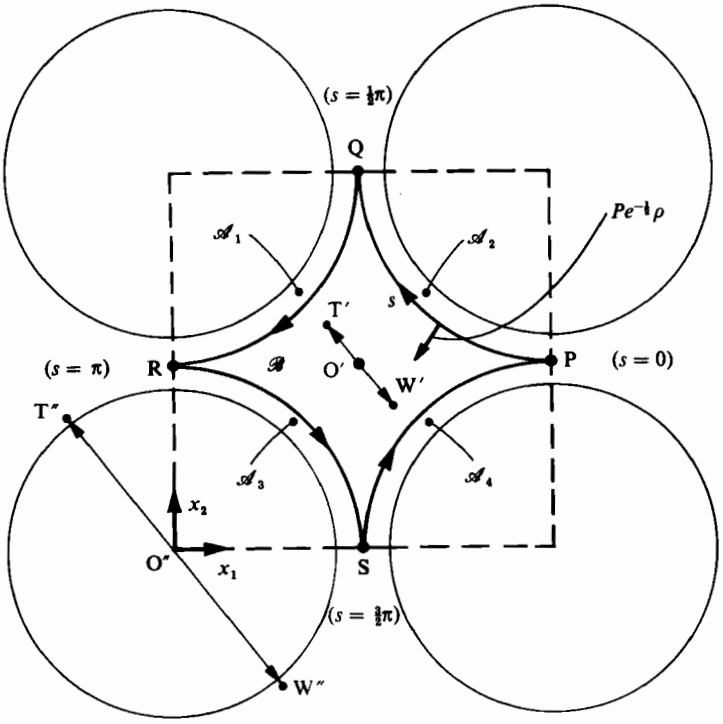

FIGURE 6. Symmetry conditions.

it suffices to determine B only for $0 \leqslant s \leqslant \pi$. In the latter domain the matching conditions implied by (6.3) and (6.5) adopt the forms

$$\lim_{\rho \to \infty} B = 1, \tag{6.8}$$

$$\lim_{\rho \to -\infty} B = 0. \tag{6.9}$$

To match the results obtained for B through the gap regions, where (6.6) does not hold continuously, we draw upon our previous observation that transport in the latter region is dominated by convection (regions $\mathscr{E}$ and $\mathscr{D}$), with B therefore constant along streamlines. Contributions from regions $\mathscr{F}$ and $\mathscr{G}$, in which diffusion plays a role, are negligible on the lengthscales $\rho \sim O(Pe^{-\frac{1}{2}})$ of interest. Thus, referring to figure 7, we obtain $B(\mathrm{U}') = B(\mathrm{U}'') = 2 - B(\mathrm{U})$, $B(\mathrm{V}') = B(\mathrm{V})$ and $B(\mathrm{W}'') = B(\mathrm{W}''') = -B(\mathrm{W}')$, in which use has been made of the symmetry conditions about points O′ and O″, along with $B(\mathrm{O}') = 1$ and $B(\mathrm{O}'') = 0$. Jump condition (4.8) further implies $B(\mathrm{T}) = B(\mathrm{T}')$ and $B(\mathrm{W}) = B(\mathrm{W}'')$. Taken together these results yield

$$B(\pi-, \rho) = 2 - B(0+, \rho) \quad (\rho > 0), \tag{6.10}$$

$$B(\pi-, \rho) = B(0+, \rho) \quad (\rho < 0), \tag{6.11}$$

$$B(\tfrac{1}{2}\pi+, \rho) = B(\tfrac{1}{2}\pi-, \rho) \quad (\rho > 0), \tag{6.12}$$

$$B(\tfrac{1}{2}\pi+, \rho) = -B(\tfrac{1}{2}\pi-, \rho) \quad (\rho < 0), \tag{6.13}$$

in the limits where the points approach the respective origins. Functions $f(a+)$ and $f(a-)$ denote the respective right and left limits of f as its argument approaches a.

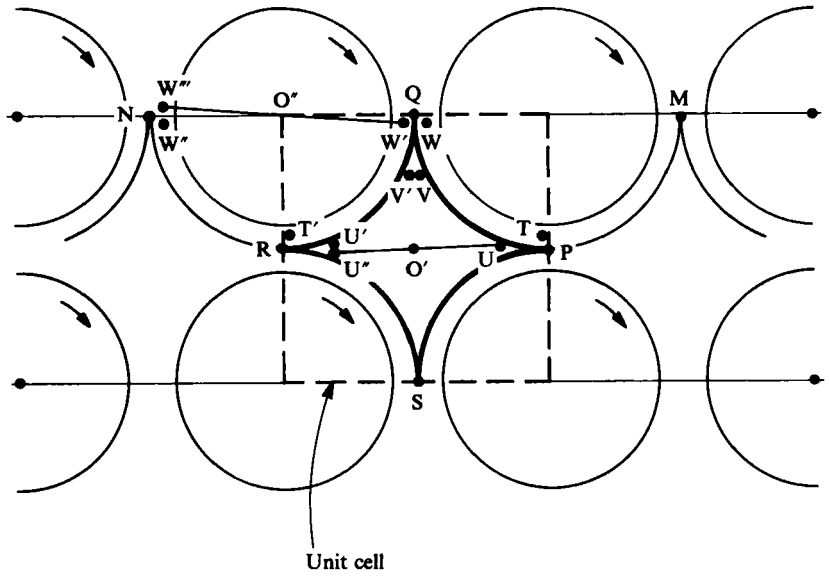

FIGURE 7. Gap continuity conditions.

Matching conditions (6.8)–(6.13) provide a complete set of conditions to determine $B(s,\rho)$ in the domain bounded by $0 \leqslant s \leqslant \pi$ and $-\infty < \rho < \infty$. It proves convenient in deriving this solution to define a quantity $\bar{B}$ which is a periodic function of s with period π. In the interval $0 \leqslant s \leqslant \pi$ it is given by

$$\bar{B}(s,\rho) = 2B(s,\rho) - 1. \tag{6.14}$$

However, outside the range $0 \leqslant s \leqslant \pi$ the value of B given by (6.14) differs from the true value of B. For instance, though for $\pi \leqslant s \leqslant \frac{3}{2}\pi$ the true value of B is that on the line RS in figure 7, the corresponding value of B given by (6.14) is that on RN.

Upon using (6.14) to write the set of equations (6.6), (6.8)–(6.13) in terms of $\bar{B}$, it is seen that the resulting equations defined on $-\infty < s < \infty$ remain invariant under the transformation $(\bar{B}; s, \rho) \rightarrow (-\bar{B}; s+\frac{1}{2}\pi, -\rho)$. Consequently

$$\bar{B}(s+\tfrac{1}{2}\pi, \rho) = -\bar{B}(s, -\rho) \quad (-\infty < s < \infty). \tag{6.15}$$

Moreover, $\bar{B}$ is everywhere continuous, except at the discontinuities depicted in figure 8, for which

$$\bar{B}(s+,\rho) = 2 - \bar{B}(s-,\rho) \quad (s = n\pi, \rho > 0) \tag{6.16}$$

and

$$\bar{B}(s+,\rho) = -2 - \bar{B}(s-,\rho) \quad (s = n\pi + \tfrac{1}{2}\pi, \rho < 0), \tag{6.17}$$

with n any integer. Equations (6.14) and (6.15) imply that

$$B(s+\tfrac{1}{2}\pi, \rho) = 1 - B(s, -\rho) \quad (0 \leqslant s \leqslant \tfrac{1}{2}\pi). \tag{6.18}$$

The latter in conjunction with (6.7) permits the solution for $\bar{B}$ (and thus B) within the subinterval $0 \leqslant s \leqslant \frac{1}{2}\pi$ to suffice for establishing B everywhere in the unit cell.

The final form of the governing transport equation within boundary layer $\mathscr{C}$ thereby becomes

$$\frac{\partial \bar{B}}{\partial s} = \frac{\partial^2 \bar{B}}{\partial \rho^2} \quad (0 \leqslant s \leqslant \tfrac{1}{2}\pi, -\infty < \rho < \infty), \tag{6.19}$$

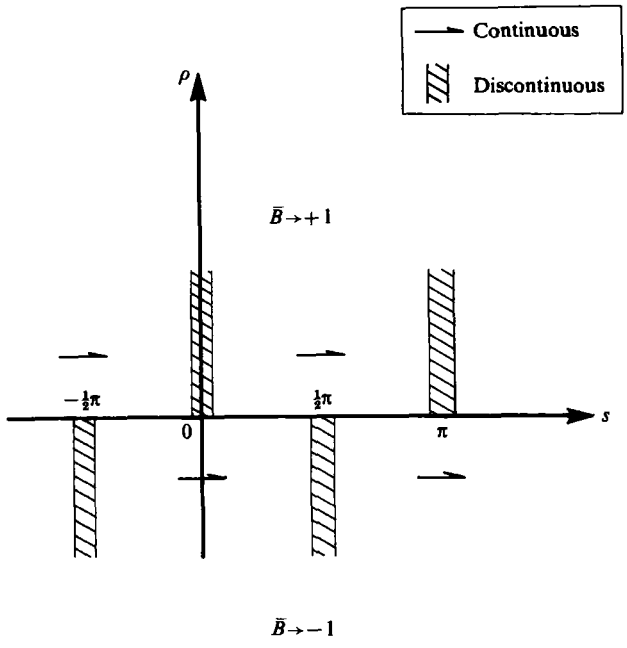

FIGURE 8. Schematical representation of discontinuities (shaded lines) in $\bar{B}$.

subject to matching conditions

$$\lim_{\rho\to\infty} \bar{B} = 1, \tag{6.20}$$

$$\lim_{\rho\to-\infty} \bar{B} = -1, \tag{6.21}$$

$$\bar{B}(0+,\rho) = 2+\bar{B}(\tfrac{1}{2}\pi-,-\rho) \quad (\rho > 0), \tag{6.22}$$

$$\bar{B}(0+,\rho) = -\bar{B}(\tfrac{1}{2}\pi-,-\rho) \quad (\rho < 0). \tag{6.23}$$

Equations (6.20) and (6.21) result directly from substitution of (6.14) into (6.8) and (6.9); (6.22) derives from (6.15) and (6.16), whereas (6.23) is a consequence of the continuity of $\bar{B}$ at $s = 0$ for $\rho < 0$, together with the result (6.15).

Matching conditions (6.20)–(6.23) uniquely determine the solution of (6.19) in the domain $0 \leqslant s \leqslant \frac{1}{2}\pi$, $-\infty < \rho < \infty$. The detailed $\bar{B}$-solution of these is derived in the following section, along with the concomitant value of the dispersion coefficient $\bar{D}^*_{22}$.

7. Solution

Equation (6.19) is formally identical to the one-dimensional heat-conduction equation with s the time-like coordinate. The Green function $G(s,\rho;s',\rho')$, defined as the solution of (6.19) at (s,ρ) for an initial Dirac delta-function disturbance $\delta(\rho-\rho')$ at $s = s'$, takes the form

$$G(s,\rho;s',\rho') = [4\pi(s-s')]^{-\frac{1}{2}} \exp\left[-\frac{(\rho-\rho')^2}{4(s-s')}\right], \tag{7.1}$$

in which $s > s'$ (as s is time-like). Define $f(\rho)$ as

$$-\bar{B}(\tfrac{1}{2}\pi-,-\rho) = f(\rho). \tag{7.2}$$

This results in

$$\bar{B}(0+,\rho) = \begin{cases} 2-f(\rho) & (\rho > 0), \\ f(\rho) & (\rho < 0), \end{cases} \tag{7.3}$$

in accordance with matching conditions (6.22) and (6.23). For $0 < s < \frac{1}{2}\pi$ the Green function (7.1) then furnishes the relation

$$\bar{B}(s,\rho) = \int_{-\infty}^{0} f(\rho')\,(4\pi s)^{-\frac{1}{2}} \exp\left[-\frac{(\rho-\rho')^2}{4s}\right] \mathrm{d}\rho' + \int_{0}^{\infty} [2-f(\rho')]\,(4\pi s)^{-\frac{1}{2}} \exp\left[-\frac{(\rho-\rho')^2}{4s}\right] \mathrm{d}\rho', \tag{7.4}$$

expressing the solution of (6.19) in terms of its 'initial' value $\bar{B}(0+,\rho)$. This equation may be rearranged into the form

$$\bar{B}(s,\rho) = 1+\phi[(4s)^{-\frac{1}{2}}\rho]-(4\pi s)^{-\frac{1}{2}}\int_{-\infty}^{\infty} f(\rho') \exp\left[-\frac{(\rho-\rho')^2}{4s}\right] \operatorname{sgn}\rho'\, \mathrm{d}\rho'. \tag{7.5}$$

When $f(\rho)$ is known this furnishes the function $\bar{B}$ everywhere within the domain of interest. In (7.5),

$$\phi(x) = \operatorname{erf} x = 2\pi^{-\frac{1}{2}}\int_{0}^{x} \exp(-\xi^2)\, \mathrm{d}\xi \tag{7.6}$$

and

$$\operatorname{sgn} x = \begin{cases} 1 & (x > 0), \\ -1 & (x < 0). \end{cases} \tag{7.7}$$

To determine $f(\rho)$ substitute (7.5) into (7.2) to obtain the integral equation

$$f(\rho) = -1+\phi[(2\pi)^{-\frac{1}{2}}\rho]+(2\pi^2)^{-\frac{1}{2}}\int_{-\infty}^{\infty} f(\rho') \exp\left[-\frac{\rho+\rho'}{2\pi}\right] \operatorname{sgn}\rho'\, \mathrm{d}\rho', \tag{7.8}$$

to be solved for $f(\rho)$ subject to the asymptotic conditions

$$\lim_{\rho\to\infty} f(\rho) = 1, \quad \lim_{\rho\to-\infty} f(\rho) = -1, \tag{7.9}$$

derived from (6.20) and (6.21). The change of variable $\rho = (2\pi)^{\frac{1}{2}}x$ together with the definition

$$2h(x) = 1-f(\rho) \tag{7.10}$$

simplifies (7.8) to the form

$$h(x)-1 = \pi^{-\frac{1}{2}}\int_{-\infty}^{\infty} h(x') \exp[-(x+x')^2] \operatorname{sgn} x'\, \mathrm{d}x', \tag{7.11}$$

which is to be solved subject to the dual requirements

$$\lim_{x\to\infty} h(x) = 0, \tag{7.12}$$

$$\lim_{x\to-\infty} h(x) = 1. \tag{7.13}$$

Equation (7.11) represents a singular, inhomogeneous, linear, Fredholm-type integral equation of the second kind. Its solution $h(x)$ eventually furnishes $\bar{B}(s,\rho)$ via (7.5) and (7.10).

To dominant order, the area A_f occurring in (5.28) is

$$A_f = [2(1+\epsilon)]^2-\pi(1)^2 \sim 4-\pi. \tag{7.14}$$

Similarly, to dominant order the integral appearing in that expression is given by

$$\int_{A_f} (\nabla B)\cdot(\nabla B)\,\mathrm{d}A \sim \int_{\text{region } \mathscr{C}} (\nabla B)\cdot(\nabla B)\,\mathrm{d}A. \tag{7.15}$$

In cylindrical polar coordinates the above integrand may be written as

$$(\partial B/\partial r)^2 + (r^{-1}\,\partial B/\partial\theta)^2$$

or equivalently, upon transformation via (5.2) and (5.3), as

$$Pe^{\frac{1}{2}}(\partial B/\partial\rho)^2 + Pe^{-\frac{1}{2}}(\partial B/\partial s)^2.$$

Neglect of terms of orders ϵ and $Pe^{-\frac{1}{2}}$ thereby yields

$$\overline{D}^*_{22} \sim (4-\pi)^{-1}\,Pe^{\frac{1}{2}}\,D\int_0^{2\pi}\mathrm{d}s\int_{-\infty}^{\infty}\mathrm{d}\rho\left(\frac{\partial B}{\partial\rho}\right)^2. \tag{7.16}$$

Equations (6.7), (6.14) and (6.15) eventually reduce the above to the form

$$\overline{D}^*_{22} \sim (4-\pi)^{-1}\,Pe^{\frac{1}{2}}\,D\int_0^{\frac{1}{2}\pi}\mathrm{d}s\int_{-\infty}^{\infty}\mathrm{d}\rho\left(\frac{\partial \overline{B}}{\partial\rho}\right)^2. \tag{7.17}$$

Integration by parts with respect to ρ, use of the governing equation (6.19), and subsequent integration by parts over s – performed successively in that order – eventually yields

$$\overline{D}^*_{22} \sim (-2)^{-1}(4-\pi)^{-1}\,Pe^{\frac{1}{2}}\,D\int_{-\infty}^{\infty}\mathrm{d}\rho\,[\overline{B}^2(\tfrac{1}{2}\pi-,\rho)-\overline{B}^2(0+,\rho)]. \tag{7.18}$$

In conjunction with (7.2), (7.3) and (7.10) the latter ultimately adopts the canonical form

$$\frac{\overline{D}^*_{22}}{D} \sim \frac{4(2\pi)^{\frac{1}{2}}\,Pe^{\frac{1}{2}}}{4-\pi}\int_0^{\infty} h(x)\,\mathrm{d}x, \tag{7.19}$$

with $h(x)$ with solution of (7.11).

Remaining components of the Taylor-dispersion dyadic may be obtained by noting that B_1 is merely a $-\frac{1}{2}\pi$ rotation about the x_3 axis of the B_2 field, i.e.

$$B_1(s,\rho) = B_2(s+\tfrac{1}{2}\pi,\rho). \tag{7.20}$$

This immediately yields $\overline{D}^*_{11} = \overline{D}^*_{22}$, whereas cross-components $\overline{D}^*_{12}$ and $\overline{D}^*_{21}$ are given by

$$\overline{D}^*_{12} = \overline{D}^*_{21} \sim D\,Pe^{\frac{1}{2}}\,A_f^{-1}\int_0^{2\pi}\mathrm{d}s\int_{-\infty}^{\infty}\mathrm{d}\rho\left(\frac{\partial B_1}{\partial\rho}\right)\left(\frac{\partial B_2}{\partial\rho}\right). \tag{7.21}$$

However, use of symmetry condition (6.7) to effect the s-integration over $(0,\pi)$, together with the facts that

$$B_1(s,\rho) = 1 - B_2(s,-\rho) \quad (0 < s < \tfrac{1}{2}\pi) \tag{7.22}$$

and

$$B_1(s,\rho) = 1 + B_2(s,-\rho) \quad (\tfrac{1}{2}\pi < s < \pi), \tag{7.23}$$

ultimately shows that

$$\overline{D}^*_{12} = \overline{D}^*_{21} = 0. \tag{7.24}$$

[Equations (7.22) and (7.23) derive by using (6.7) and (6.18) in conjunction with (7.20).]

Finally, the B_3 component of the microfield $\boldsymbol{B}$ can be determined by arbitrarily

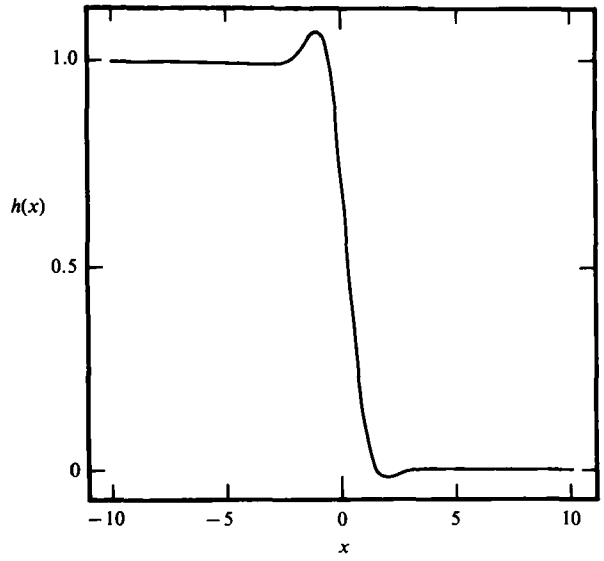

FIGURE 9. Solution $h(x)$ of integral equation (7.11) satisfying (7.12) and (7.13).

selecting a cell of unit length in the x_3 direction. It is straightforwardly demonstrated that the latter possesses the solution

$$B_3 = -x_3 \tag{7.25}$$

to within an arbitrary additive constant. This yields

$$\overline{D}^*_{33} = \frac{D}{\tau_f}\int_{\tau_f} \nabla B_3 \cdot \nabla B_3 \, \mathrm{d}\boldsymbol{r} \equiv D \tag{7.26}$$

and

$$\overline{D}^*_{13} = \overline{D}^*_{31} = \overline{D}^*_{23} = \overline{D}^*_{32} = 0. \tag{7.27}$$

The foregoing results show the Taylor-dispersivity dyadic to be transversely isotropic, and hence of the generic form

$$\overline{\boldsymbol{D}}^* \sim \overline{D}^*_{\parallel} \boldsymbol{i}_3 \boldsymbol{i}_3 + \overline{D}^*_{\perp}(\boldsymbol{I} - \boldsymbol{i}_3 \boldsymbol{i}_3), \tag{7.28}$$

with $\boldsymbol{i}_3$ a unit vector parallel to the cylinder axes and $\boldsymbol{I}$ the dyadic idemfactor. Respective components parallel and transverse to the axes possess the asymptotic forms

$$\overline{D}^*_{\parallel}/D = 1 \tag{7.29}$$

and

$$\frac{\overline{D}^*_{\perp}}{D} = \frac{4(2\pi)^{\frac{1}{2}} Pe^{\frac{1}{2}}}{4-\pi}\int_0^\infty h(x)\,\mathrm{d}x \tag{7.30}$$

in the dual limits $Pe \to \infty$ and $\epsilon \to 0$, with $Pe\,\epsilon^2 \gg 1$. That the Taylor dispersivity is transversely isotropic is evident from symmetry considerations.

To derive the requisite numerical coefficient in (7.30), the integral equation (7.11) was solved numerically (Nadim 1984) for $h(x)$, resulting in the functional dependence displayed in figure 9. Numerical integration of these data subsequently gave $\int_0^\infty h(x)\,\mathrm{d}x = 0.3766$, leading to the expression

$$\overline{D}^*_{\perp}/D = 4.40\, Pe^{\frac{1}{2}}. \tag{7.31}$$

Extension of the above analysis to encompass the more general case where the cylinders (solid phase) are themselves conductors is carried out in the next section.

8. Non-zero solid-phase diffusivity

Denote by κ the solid/fluid diffusivity ratio D^s/D. For times exceeding

$$\max(R^2/D, R^2/D^s)$$

the Taylor dispersivity may be calculated from (3.4) jointly with (3.5) to (3.10). In the limit $\kappa \to 0$, (3.4) remains properly normalized for 'long' times ($t \gg R^2/D^s$), whereas the result obtained in the previous section (based on the normalization $1/\tau_f$) can be interpreted as the proper 'short-time' solution ($R^2/D \ll t \ll R^2/D^s$).

As B = constant satisfies the governing solid-phase equation (3.6) and boundary condition (3.8) in the limit $Pe\,\epsilon^2 \gg 1$, the previous solution remains valid with B adopting the same constant values within the cylinders as in regions $\mathscr{A}_1$–$\mathscr{A}_4$. [Refer to figure 6 and (6.3), (6,4).] Consequently, with proper normalization it is found that

$$\overline{D}^*_{\parallel} = \tau_0^{-1}(D\tau_f + D^s\tau_s) = D[1 + (\kappa - 1)\tfrac{1}{4}\pi] \tag{8.1}$$

and, in the $Pe\,\epsilon^2 \gg 1$ limit,

$$\overline{D}^*_{\perp} = (2\pi\, Pe)^{\frac{1}{2}} D \int_0^\infty h(x)\,\mathrm{d}x = 0.944\, Pe^{\frac{1}{2}} D. \tag{8.2}$$

As before, $h(x)$ is the solution of (7.11).

Suppose that, while $Pe \to \infty$ and $\epsilon \to 0$, $Pe\,\epsilon^2 = O(1)$ rather than (5.5). In these altered circumstances bondary-layer regions $\mathscr{C}$ no longer remain distant from the cylinder surfaces. Regions $\mathscr{A}_1$–$\mathscr{A}_4$ then withdraw into the solid phase, whereupon flux boundary condition (3.8) can no longer be satisfied by taking B = constant within the cylinders. In the degenerate case $\kappa = 1$, however, the solid- and fluid-transport equations become identical, whence the same governing set of equations and boundary conditions now obtain in regions $\mathscr{C}$ as in the preceding section. Therefore, in the limit $Pe\,\epsilon^2 \sim O(1)$ with $\kappa = 1$, (8.1) and (8.2) are once again obtained for the parallel and transverse dispersivity components.

These limiting cases prove useful in establishing the consistency of the subsequent $Pe\,\epsilon^2 \sim O(1)$ solution for a general value of κ. Moreover, (8.2) is of further interest in establishing that the transverse dispersivity component is independent of D^s in the limit $Pe\,\epsilon^2 \gg 1$.

Consider the situation $Pe\,\epsilon^2 \sim O(1)$ with κ arbitrary. Insofar as the Péclet number based upon the solid-phase diffusivity simultaneously remains large (i.e. $Pe/\kappa \gg 1$), the dominant contribution to the Taylor dispersivity again arises from regions $\mathscr{C}$ (see table 1). We further require that $Pe\,\epsilon^2$ be much larger than ϵ (i.e. $Pe\,\epsilon \gg 1$) since otherwise contributions from domains $\mathscr{E}$ and $\mathscr{G}$ will become comparable to or larger than that from $\mathscr{C}$. The definition $\overline{B} = 2B - 1$ thereby yields the following transformed set of differential equations and matching conditions, in analogy with results derived previously:

$$\frac{\partial^2 \overline{B}}{\partial \rho^2} = \frac{\partial \overline{B}}{\partial s} \quad (\rho > -\rho^*), \tag{8.3}$$

$$\kappa \frac{\partial^2 \overline{B}}{\partial \rho^2} = \frac{\partial \overline{B}}{\partial s} \quad (\rho < -\rho^*), \tag{8.4}$$

$$\lim_{\rho \to \infty} \overline{B} = 1, \tag{8.5}$$

$$\lim_{\rho \to -\infty} \overline{B} = -1, \tag{8.6}$$

$G(s,\rho;s',\rho') = [4\pi(s-s')]^{-\frac{1}{2}}\{a\exp[-(\rho-\rho')^2/4c(s-s')]+b\exp[-(d\rho+e\rho'+fPe^{\frac{1}{2}}\epsilon)^2/4c(s-s')]\}$

Domains	Coefficient a	b	c	d	e	f
$\rho'>-\rho^*$ and $\rho>-\rho^*$,	1	$\frac{1-\kappa^{\frac{1}{2}}}{1+\kappa^{\frac{1}{2}}}$	1	1	1	1
$\rho'>-\rho^*$ and $\rho<-\rho^*$,	0	$\frac{2}{1+\kappa^{\frac{1}{2}}}$	1	$\kappa^{-\frac{1}{2}}$	-1	$\frac{1-\kappa^{\frac{1}{2}}}{2\kappa^{\frac{1}{2}}}$
$\rho'<-\rho^*$ and $\rho>-\rho^*$,	0	$\frac{2}{1+\kappa^{\frac{1}{2}}}$	1	1	$-\kappa^{-\frac{1}{2}}$	$\frac{\kappa^{\frac{1}{2}}-1}{2\kappa^{\frac{1}{2}}}$
$\rho'<-\rho^*$ and $\rho<-\rho^*$,	$\kappa^{-\frac{1}{2}}$	$\frac{\kappa^{\frac{1}{2}}}{\kappa^{\frac{1}{2}}(1+\kappa^{\frac{1}{2}})}$	κ	1	1	1

TABLE 2. Green function for equations (8.3)–(8.4) satisfying equations (8.7)–(8.8)

$$\left.\begin{aligned}\overline{B}\text{ continuous},\\ (\kappa\partial\overline{B}/\partial\rho)_s = (\partial\overline{B}/\partial\rho)_f\end{aligned}\right\} \quad (\rho=-\rho^*), \tag{8.7, 8.8}$$

$$\overline{B}(\tfrac{1}{2}\pi+,\rho) = \overline{B}(\tfrac{1}{2}\pi-,\rho) \quad (\rho>0), \tag{8.9}$$

$$\overline{B}(\tfrac{1}{2}\pi+,\rho) = -2-\overline{B}(\tfrac{1}{2}\pi-,\rho) \quad (\rho<0), \tag{8.10}$$

$$\overline{B}(0+,\rho) = \overline{B}(\pi-,\rho) \quad (\rho<0), \tag{8.11}$$

$$\overline{B}(0+,\rho) = 2-\overline{B}(\pi-,\rho) \quad (\rho>0). \tag{8.12}$$

Here
$$\rho^* = \tfrac{1}{2}(Pe\,\epsilon^2)^{\frac{1}{2}}, \tag{8.13}$$

so that $\rho=-\rho^*$ denotes the cylinder surfaces (8.13) [cf. (5.2)].

Insofar as condition (6.7) remains valid, we need only solve for $\overline{B}$ in the domain $0\leqslant s\leqslant\pi$. However, the invariance result (6.15) no longer obtains [since (8.8) does not transform into itself under the latter transformation]. As such it is not possible to further restrict the calculations to the region $0\leqslant s\leqslant\frac{1}{2}\pi$, as was previously done. Such minor technical differences notwithstanding, however, subsequent steps of the present solution are completely akin to prior calculations for the $\kappa=0$ case.

The Green function $G(s,\rho;s',\rho')$ satisfying (8.3) and (8.4) together with (8.7) and (8.8) may be found by the method of images (Appendix A), the result being tabulated in table 2. Define

$$\overline{B}(0-,\rho) = f(\rho) \tag{8.14}$$

and recall the π-periodicity result

$$\overline{B}(\pi-,\rho) = \overline{B}(0-,\rho) = f(\rho) \tag{8.15}$$

to obtain

$$\overline{B}(0+,\rho) = \begin{cases}2-f(\rho) & (\rho>0),\\ f(\rho) & (\rho<0),\end{cases} \tag{8.16}$$

corresponding to (8.11) and (8.12). With $\bar{B}(0+,\rho)$ given in terms of $f(\rho)$ via (8.16), the Green function furnishes the relation

$$\bar{B}(\tfrac{1}{2}\pi-,\rho) = \int_{-\infty}^{\infty} \bar{B}(0+,\rho')\, G(\tfrac{1}{2}\pi,\rho;0,\rho')\,\mathrm{d}\rho'. \tag{8.17}$$

Applying gap conditions (8.9) and (8.10) to the latter provides $\bar{B}(\frac{1}{2}\pi+,\rho)$. In turn, this renders $\bar{B}(\pi-,\rho)$ expressible as

$$\bar{B}(\pi-,\rho) = \int_{-\infty}^{\infty} \bar{B}(\tfrac{1}{2}\pi+,\rho'')\, G(\pi,\rho;\tfrac{1}{2}\pi,\rho'')\,\mathrm{d}\rho''. \tag{8.18}$$

Inasmuch as the right-hand side of (8.18) can be written as an integral functional of $f(\rho)$, the π-periodicity requirement (8.15) provides an integral equation for $f(\rho)$. Explicitly, define the three functions

$$I_1(\rho) = \int_{-\infty}^{0} G(\pi,\rho;\tfrac{1}{2}\pi,\rho'')\,\mathrm{d}\rho'', \tag{8.19}$$

$$I_2(\rho,\rho') = \int_{-\infty}^{0} G(\pi,\rho;\tfrac{1}{2}\pi,\rho'')\, G(\tfrac{1}{2}\pi,\rho'';0,\rho')\,\mathrm{d}\rho'', \tag{8.20}$$

$$I_3(\rho,\rho') = \int_{0}^{\infty} G(\pi,\rho;\tfrac{1}{2}\pi,\rho'')\, G(\tfrac{1}{2}\pi,\rho'';0,\rho')\,\mathrm{d}\rho'', \tag{8.21}$$

and introduce the transformation $g(\rho) = f(\rho) - 1$ to obtain

$$g(\rho) + 2I_1(\rho) + 1 = \int_{-\infty}^{\infty} [1 - g(\rho')\,\operatorname{sgn}\rho']\,[I_3(\rho,\rho') - I_2(\rho,\rho')]\,\mathrm{d}\rho'. \tag{8.22}$$

The latter constitutes an integral equation for $g(\rho)$. Despite its more complex form, it is of precisely the same type as encountered previously [cf. (7.11)]. In consequence of matching conditions (8.5) and (8.6), the two limiting conditions

$$\lim_{\rho\to\infty} g(\rho) = 0, \tag{8.23}$$

$$\lim_{\rho\to-\infty} g(\rho) = -2, \tag{8.24}$$

need to be imposed. The functional forms of the integrals defined in (8.19)–(8.21) have been obtained explicitly from table 2. They are tabulated in Appendix B. In view of the dependence of the Green function (table 2) upon parameters κ and ρ^*, I_1–I_3 also exhibit such dependence.

In analogy with (7.15)–(7.17) the transverse component of the Taylor-dispersivity dyadic here takes the form

$$\frac{\bar{D}_\perp^*}{D} = \tfrac{1}{8} Pe^2 \int_0^{\pi} \mathrm{d}s \left[\int_{-\infty}^{-\rho^*} \kappa \left(\frac{\partial \bar{B}}{\partial \rho}\right)^2 \mathrm{d}\rho + \int_{-\rho^*}^{\infty} \left(\frac{\partial \bar{B}}{\partial \rho}\right)^2 \mathrm{d}\rho \right]. \tag{8.25}$$

Several integrations by parts in conjunction with (8.3), (8.4) and (8.8) eventually render the right-hand side of (8.25) expressible explicitly in terms of $f(\rho)$. The transformation $g(\rho) = f(\rho) - 1$ together with the demonstrable fact that

$$\int_{-\infty}^{0} G(\tfrac{1}{2}\pi,\rho';0,\rho)\,\mathrm{d}\rho' = I_1(\rho) \tag{8.26}$$

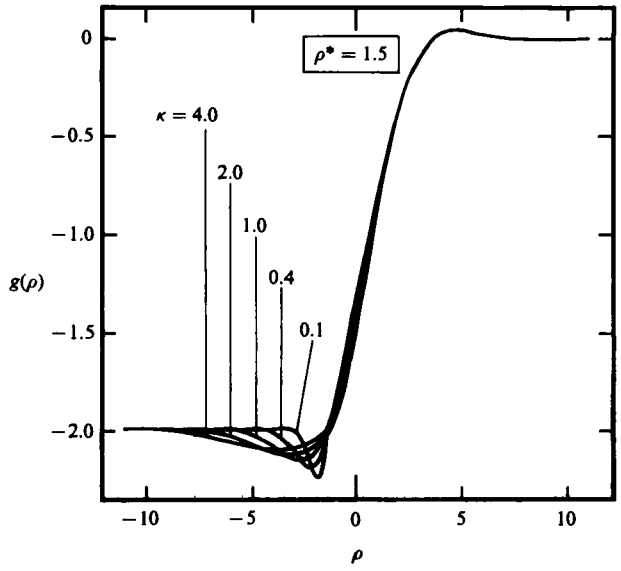

FIGURE 10. Solution $g(\rho)$ of integral equation (8.22) satisfying (8.23) and (8.24).

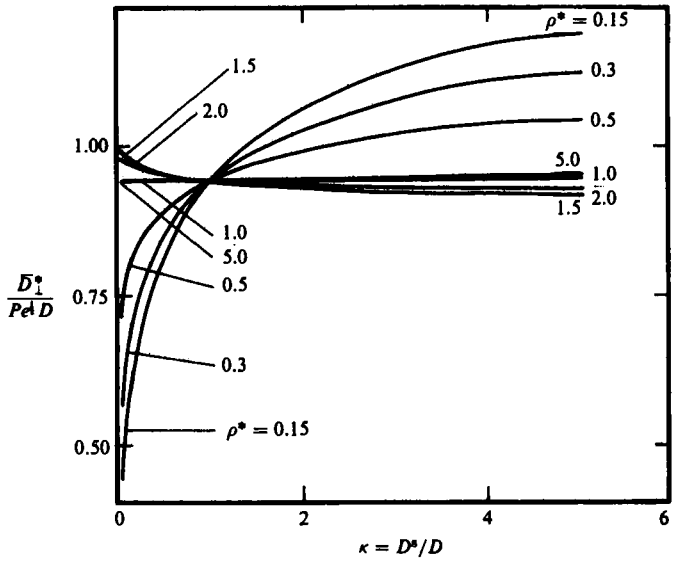

FIGURE 11. Transverse dispersivity as a function of κ at parameters of ρ^*.

[deriving from the dual conditions that $G(\frac{1}{2}\pi+\hat{s},\rho';\hat{s},\rho)$ is independent of $\hat{s}$ and $G(\frac{1}{2}\pi,\rho';0,\rho) = G(\frac{1}{2}\pi,\rho;0,\rho')$], then yields the final expression

$$\frac{\bar{D}_\perp^*}{D} = \frac{Pe^{\frac{1}{2}}}{4}\left\{\int_{-\infty}^{\infty}[2-g(\rho)\operatorname{sgn}\rho]\,I_1(\rho)\,\mathrm{d}\rho - \int_0^{\infty} g(\rho)\,\mathrm{d}\rho\right\}. \tag{8.27}$$

Together with the relation

$$\frac{\bar{D}_\parallel^*}{D} = [1+(\kappa-1)\tfrac{1}{4}\pi] \tag{8.28}$$

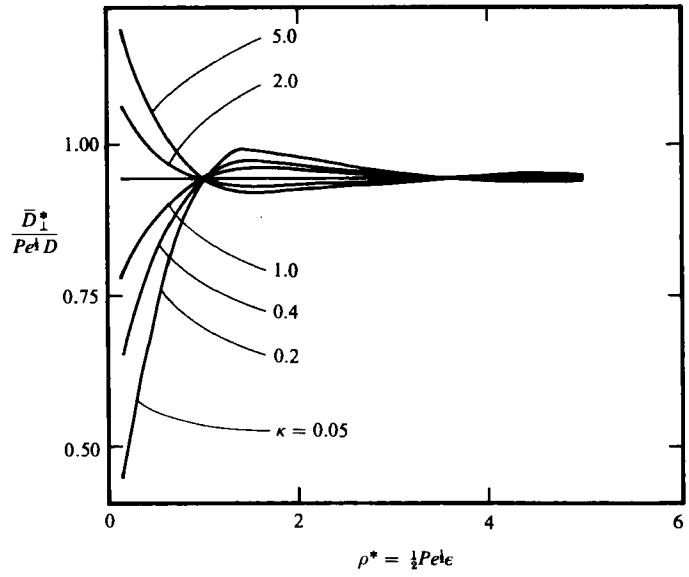

FIGURE 12. Transverse dispersivity as a function of ρ^* at parameters of κ.

these furnish the transverse and parallel components of the macroconductivity dyadic (7.28) for the case $Pe\,\epsilon^2 \sim O(1)$ and arbitrary κ. The dependence of (8.27) upon the two parameters κ and ρ^* is implicit in the functional dependence of both $I_1(\rho)$ and $g(\rho)$ upon each of these.

Subject to auxiliary conditions (8.23) and (8.24), the solution $g(\rho)$ of the integral equation (8.22) was effected (Nadim 1984) by numerical means in the parametric ranges $0.05 \leqslant \kappa \leqslant 5$ and $0.15 \leqslant \rho^* \leqslant 5.0$. In conjunction with (8.13) the latter corresponds to $0.09 \leqslant Pe\,\epsilon^2 \leqslant 100$. Typical solutions $g(\rho)$ are depicted in figure 10 for several parametric choices. Subsequent integration eventually provided the coefficient required in (8.27). Numerical values of $\bar{D}_\perp^*/D\,Pe^{\frac{1}{2}}$ are shown in figures 11 and 12 as functions of parameters κ and ρ^*. Results for the two limiting cases $\kappa = 1$ and $Pe\,\epsilon^2 \to \infty$ (i.e. $\rho^* \to \infty$) obviously accord with the prior result (8.2).

9. Discussion

Consistent with the absence of flow at the macroscale [cf. (3.1)], steady-state heat transfer in the suspension of rotating cylinders is constitutively described by a Fourier-type conduction equation possessing a macroconductivity dyadic $\bar{\boldsymbol{D}}^*$. Though macroconvection as a formal heat-transfer mechanism is absent in this example, microconvection effects arising from the interstitial fluid motion are nevertheless implicitly evidenced through the dependence of the conductivity dyadic upon the internal rotary Péclet number. Indeed, measurements of $\bar{D}_\perp^*$ offer a possible way of indirectly measuring the relative suspension-particle internal spin rate Ω. Knowledge of this difficult-to-measure kinematical variable is important in rheological theories of so-called micropolar fluids (Eringen 1964, 1966; pertinent literature up to 1984 is reviewed by Brenner 1984).

That the transverse conductivity $\bar{D}_\perp^*$ is functionally dependent upon Ω has several implications. First, as described above, since internal particle rotation is not a directly observable kinematic property, such reference-frame-dependent transport

measurements provide an *indirect* way of measuring Ω. Even in the absence of a quantitative theory such as that outlined above, the mere existence of a functional dependence is *prima facie* evidence of the polarizable nature of the macrocontinuum. Furthermore, since the effective conductivity of such a polar suspension can obviously be varied at will by merely changing the rotation speed of the apparatus housing the suspension (Brenner 1984), applications are easily envisioned in which the same medium can play opposite roles as insulator or conductor according to needs.

In addition to displaying unusual heat- and mass-transfer characteristics, our dipolar suspension exhibits equally striking momentum-transfer properties in the form of antisymmetric stresses (Brenner 1970, 1972; Brenner & Weissman 1972; Brenner & Condiff 1974; Jansons 1983; Brenner 1984). In particular, Cauchy's moment-of-momentum equation (Dahler & Scriven 1961, 1963; Aris 1962) for the microstress tensor $\boldsymbol{T}$ here adopts the degenerate form (Brenner 1970, Brenner & Weissman 1972)

$$\boldsymbol{T}_{\times} + \boldsymbol{G} = \boldsymbol{0}, \tag{9.1}$$

corresponding to the neglect of rotary inertial effects and the absence of couple-stress effects (Condiff & Dahler 1964)). Absence of the latter is a consequence of the prevailing geometric and kinematic homogeneity at the macroscale. Here $\boldsymbol{G}$ is the volumetric external body-couple density, and $\boldsymbol{T}_{\times} = -\boldsymbol{\epsilon}:\boldsymbol{T}$ the pseudovector invariant of the suspension-scale stress tensor; $\boldsymbol{\epsilon}$ is the unit alternating isotropic triadic (ϵ_{jkl}).

The existence of body couples reflects the torques supplied by an external agency to the cylindrical particles, such torques being required to maintain these particles in a state of permanent rotation. In the limit $\epsilon \to 0$ a lubrication-theory estimate is easily found for the hydrodynamic couple (per unit length in x_3 direction) exerted by the fluid on each cylinder. The latter is necessarily equal in magnitude and opposite to the couple supplied by the external agency. Thus, for particles rotating in the chiral sense depicted in figure 3, the external couple $\boldsymbol{L}$ (per unit length) acting upon an individual cylinder is

$$\boldsymbol{L} \sim -\boldsymbol{i}_3 4\pi \left(\frac{2}{\epsilon}\right)^{\frac{1}{2}} \mu R^2 \Omega. \tag{9.2}$$

Division by the area $4R^2$ of a unit cell (containing one particle) yields

$$\boldsymbol{G} \sim -\boldsymbol{i}_3 \pi \left(\frac{2}{\epsilon}\right)^{\frac{1}{2}} \mu \Omega \tag{9.3}$$

as the external body-couple density per unit volume.

The spin viscosity ζ is defined as the phenomenological coefficient appearing in the linear constitutive equation (Condiff & Dahler 1964)

$$\boldsymbol{T}_{\times} = \zeta(\boldsymbol{\omega} - \boldsymbol{\Omega}), \tag{9.4}$$

with $\boldsymbol{\omega} = \frac{1}{2}(\nabla \times \boldsymbol{v})$, half the suspension-scale vorticity pseudovector (relative to the same observer measuring $\boldsymbol{\Omega}$), and $\boldsymbol{\Omega}$ the internal spin field, given by $\boldsymbol{\Omega} = -\boldsymbol{i}_3 \Omega$. Thus, if we observe that in our prototype example the suspension-scale velocity is zero (requiring that $\boldsymbol{\omega} = \boldsymbol{0}$), we obtain from (9.1), (9.3) and (9.4) the expression

$$\zeta = \pi \left(\frac{2}{\epsilon}\right)^{\frac{1}{2}} \mu \tag{9.5}$$

for the spin-viscosity coefficient in the lubrication limit. Similar estimates are available (Zuzovsky, Adler & Brenner 1983) for comparably concentrated *spherical*-particle suspensions.

The symmetric portion of the suspension-scale deviatoric stress tensor $\boldsymbol{T}$ is zero in the present case, whence the macrostress is purely antisymmetric. That any stress whatsoever exists in a mobile continuum 'at rest' is remarkable, much less that this is antisymmetric. As discussed by Brenner (1984) this further implies, *inter alia*, that a net couple must also be exerted by the container walls bounding the suspension, and that this wall couple must be equal in magnitude and opposite in direction to the sum of all the external couples acting upon the microscopic particles.

During this research R.G.C. was on sabbatical leave from McGill University. He wishes to thank the Chemical Engineering Department at M.I.T. for their hospitality during his stay.

Appendix A

In accordance with (8.3) and (8.4) we seek the steady spatial distribution $\bar{B}$ resulting from a unit disturbance at (s', ρ') satisfying (8.7) and (8.8). To that end introduce the changes of variable

$$\tilde{\rho} = \begin{cases} \rho + \rho^* & (\rho > -\rho^*), \quad \text{(A 1)} \\ \kappa^{-\frac{1}{2}}(\rho + \rho^*) & (\rho < -\rho^*). \quad \text{(A 2)} \end{cases}$$

This transforms both (8.3) and (8.4) into the form

$$\frac{\partial \bar{B}}{\partial s} = \frac{\partial^2 \bar{B}}{\partial \tilde{\rho}^2} \quad (\forall \tilde{\rho}). \tag{A 3}$$

Conditions (8.7) and (8.8) now take the forms

$$\bar{B} \text{ continuous} \quad (\tilde{\rho} = 0) \tag{A 4}$$

and

$$\left(\kappa^{\frac{1}{2}} \frac{\partial \bar{B}}{\partial \tilde{\rho}}\right)_s = \left(\frac{\partial \bar{B}}{\partial \tilde{\rho}}\right)_f \quad (\tilde{\rho} = 0), \tag{A 5}$$

where $\tilde{\rho} = 0$ corresponds to the position of the fluid–solid interface.

Equation (A 3) is formally identical with the one-dimensional heat-conduction equation. For the case where the unit source is at $\tilde{\rho}' > 0$ the fundamental solution is

$$\bar{B}(s, \tilde{\rho}) = \begin{cases} \alpha(s-s')^{-\frac{1}{2}} \exp\left[-\dfrac{(\tilde{\rho}-\tilde{\rho}')^2}{4(s-s')}\right] + \beta(s-s')^{-\frac{1}{2}} \exp\left[-\dfrac{(\tilde{\rho}+\tilde{\rho}')^2}{4(s-s')}\right] & (\tilde{\rho} > 0), \quad \text{(A 6)} \\ \gamma(s-s')^{-\frac{1}{2}} \exp\left[-\dfrac{(\tilde{\rho}-\tilde{\rho}')^2}{4(s-s')}\right] & (\tilde{\rho} < 0). \quad \text{(A 7)} \end{cases}$$

The second term in (A 6) arises from an image source at $\tilde{\rho} = -\tilde{\rho}'$.

Conditions (A 4) and (A 5) require that

$$\alpha + \beta = \gamma, \tag{A 8}$$

$$\alpha - \beta = \kappa^{\frac{1}{2}} \gamma, \tag{A 9}$$

which together yield

$$\beta = (1 - \kappa^{\frac{1}{2}})(1 + \kappa^{\frac{1}{2}})^{-1} \alpha \tag{A 10}$$

and

$$\gamma = 2(1 + \kappa^{\frac{1}{2}})^{-1} \alpha. \tag{A 11}$$

Normalization ($\int_{-\infty}^{\infty} \bar{B}(s,\rho)\,\mathrm{d}\rho = 1$) requires that

$$\alpha = (4\pi)^{-\frac{1}{2}}. \tag{A 12}$$

Substitute into (A 6) and (A 7) the coefficients (A 12), (A 10) and (A 11), and use transformations (A 1) and (A 2) to obtain the entries appearing in the first two rows of table 2. For the case $\tilde{\rho}'' < 0$ a similar development furnishes the coefficients appearing in the remaining rows of that table.

Appendix B

$$I_1(\rho) = \int_{-\infty}^{0} G(\pi,\rho;\tfrac{1}{2}\pi,\rho'')\,\mathrm{d}\rho''$$

$\rho > -\rho^*$,	$\frac{\kappa^{\frac{1}{2}}}{1+\kappa^{\frac{1}{2}}} - \frac{1}{2}\phi\left[\frac{\rho}{(2\pi)^{\frac{1}{2}}}\right] + \frac{1-\kappa^{\frac{1}{2}}}{2(1+\kappa^{\frac{1}{2}})}\,\phi\left[\frac{\rho+2\rho^*}{(2\pi)^{\frac{1}{2}}}\right]$;
$\rho < -\rho^*$,	$\frac{\kappa^{\frac{1}{2}}}{1+\kappa^{\frac{1}{2}}} - \frac{1}{1+\kappa^{\frac{1}{2}}}\,\phi\left[\frac{\rho+(1-\kappa^{\frac{1}{2}})\rho^*}{(2\kappa\pi)^{\frac{1}{2}}}\right]$.

TABLE 3. Integral $(-\infty, 0)$ of Green function. $\phi(x)$ is the error function given by (7.6).

$$I_2(\rho,\rho') = \int_{-\infty}^{0} G(\pi,\rho;\tfrac{1}{2}\pi,\rho'')\,G(\tfrac{1}{2}\pi,\rho'';0,\rho')\,\mathrm{d}\rho''$$

$\rho > -\rho^*$ and $\rho' > -\rho^*$,	$\frac{1}{4\pi}\exp\left[\frac{-(\rho-\rho')^2}{4\pi}\right]\left[\frac{4\kappa^{\frac{1}{2}}}{(1+\kappa^{\frac{1}{2}})^2} - \phi\left(\frac{\rho+\rho'}{2\pi^{\frac{1}{2}}}\right) + \left(\frac{1-\kappa^{\frac{1}{2}}}{1+\kappa^{\frac{1}{2}}}\right)^2 \phi\left(\frac{\rho+\rho'+4\rho^*}{2\pi^{\frac{1}{2}}}\right)\right]$ $+\frac{1}{4\pi}\left(\frac{1-\kappa^{\frac{1}{2}}}{1+\kappa^{\frac{1}{2}}}\right)\exp\left[\frac{-(\rho+\rho'+2\rho^*)^2}{4\pi}\right]\left[\phi\left(\frac{\rho-\rho'+2\rho^*}{2\pi^{\frac{1}{2}}}\right)+\phi\left(\frac{\rho'-\rho+2\rho^*}{2\pi^{\frac{1}{2}}}\right)\right]$;
$\rho > -\rho^*$ and $\rho' < -\rho^*$,	$\frac{1}{2\pi(1+\kappa^{\frac{1}{2}})}\exp\left\{\frac{-[\rho'-\kappa^{\frac{1}{2}}\rho+(1-\kappa^{\frac{1}{2}})\rho^*]^2}{4\pi\kappa}\right\}\left[1-\phi\left(\frac{\rho'+\kappa^{\frac{1}{2}}\rho+(1-\kappa^{\frac{1}{2}})\rho^*}{2(\kappa\pi)^{\frac{1}{2}}}\right)\right]$ $+\frac{1-\kappa^{\frac{1}{2}}}{2\pi(1+\kappa^{\frac{1}{2}})^2}\exp\left\{\frac{-[\rho'+\kappa^{\frac{1}{2}}\rho+(1+\kappa^{\frac{1}{2}})\rho^*]^2}{4\kappa\pi}\right\}\left[\phi\left(\frac{\kappa^{\frac{1}{2}}\rho-\rho'-(1-3\kappa^{\frac{1}{2}})\rho^*}{2(\kappa\pi)^{\frac{1}{2}}}\right)-1\right]$;
$\rho < -\rho^*$ and $\rho' > -\rho^*$,	$\frac{1}{2\pi(1+\kappa^{\frac{1}{2}})}\exp\left\{\frac{-[\rho-\kappa^{\frac{1}{2}}\rho'+(1-\kappa^{\frac{1}{2}})\rho^*]^2}{4\kappa\pi}\right\}\left[1-\phi\left(\frac{\rho+\kappa^{\frac{1}{2}}\rho'+(1-\kappa^{\frac{1}{2}})\rho^*}{2(\kappa\pi)^{\frac{1}{2}}}\right)\right]$ $+\frac{1-\kappa^{\frac{1}{2}}}{2\pi(1+\kappa^{\frac{1}{2}})^2}\exp\left\{\frac{-[\rho+\kappa^{\frac{1}{2}}\rho'+(1+\kappa^{\frac{1}{2}})\rho^*]^2}{4\kappa\pi}\right\}\left[\phi\left(\frac{\kappa^{\frac{1}{2}}\rho'-\rho-(1-3\kappa^{\frac{1}{2}})\rho^*}{2(\kappa\pi)^{\frac{1}{2}}}\right)-1\right]$;
$\rho < -\rho^*$ and $\rho' < -\rho^*$,	$\frac{1}{4\pi\kappa^{\frac{1}{2}}}\exp\left[\frac{-(\rho-\rho')^2}{4\kappa\pi}\right]\left[\frac{2(1+\kappa)}{(1+\kappa^{\frac{1}{2}})^2} - \frac{4\kappa^{\frac{1}{2}}}{(1+\kappa^{\frac{1}{2}})^2}\,\phi\left(\frac{\rho+\rho'+2(1-\kappa^{\frac{1}{2}})\rho^*}{2(\kappa\pi)^{\frac{1}{2}}}\right)\right]$ $-\frac{1-\kappa^{\frac{1}{2}}}{2\pi\kappa^{\frac{1}{2}}(1+\kappa^{\frac{1}{2}})}\exp\left[\frac{-(\rho+\rho'+2\rho^*)^2}{4\kappa\pi}\right]$.

TABLE 4. Integral $(-\infty, 0)$ of a product of Green functions

$$I_3(\rho,\rho') = \int_0^\infty G(\pi,\rho;\tfrac{1}{2}\pi,\rho'')\,G(\tfrac{1}{2}\pi,\rho'';0,\rho')\,\mathrm{d}\rho''$$

$\rho > -\rho^*$ and $\rho' > -\rho^*$,	$\frac{1}{4\pi}\exp\left[\frac{-(\rho-\rho')^2}{4\pi}\right]\left[\frac{2(1+\kappa)}{(1+\kappa^{\frac{1}{2}})^2}+\phi\left(\frac{\rho+\rho'}{2\pi^{\frac{1}{2}}}\right)-\left(\frac{1-\kappa^{\frac{1}{2}}}{1+\kappa^{\frac{1}{2}}}\right)^2\phi\left(\frac{\rho+\rho'+4\rho^*}{2\pi^{\frac{1}{2}}}\right)\right]$ $+\frac{1}{4\pi}\left(\frac{1-\kappa^{\frac{1}{2}}}{1+\kappa^{\frac{1}{2}}}\right)\exp\left[\frac{-(\rho+\rho'+2\rho^*)^2}{4\pi}\right]\left[2-\phi\left(\frac{\rho-\rho'+2\rho^*}{2\pi^{\frac{1}{2}}}\right)-\phi\left(\frac{\rho'-\rho+2\rho^*}{2\pi^{\frac{1}{2}}}\right)\right];$
$\rho > -\rho^*$ and $\rho' < -\rho^*$,	$\frac{1}{2\pi(1+\kappa^{\frac{1}{2}})}\exp\left\{\frac{-[\rho'-\kappa^{\frac{1}{2}}\rho+(1-\kappa^{\frac{1}{2}})\rho^*]^2}{4\kappa\pi}\right\}\left[1+\phi\left(\frac{\rho'+\kappa^{\frac{1}{2}}\rho+(1-\kappa^{\frac{1}{2}})\rho^*}{2(\kappa\pi)^{\frac{1}{2}}}\right)\right]$ $+\frac{1-\kappa^{\frac{1}{2}}}{2\pi(1+\kappa^{\frac{1}{2}})^2}\exp\left\{\frac{-[\rho'+\kappa^{\frac{1}{2}}\rho+(1+\kappa^{\frac{1}{2}})\rho^*]^2}{4\kappa\pi}\right\}\left[1-\phi\left(\frac{\kappa^{\frac{1}{2}}\rho-\rho'-(1-3\kappa^{\frac{1}{2}})\rho^*}{2(\kappa\pi)^{\frac{1}{2}}}\right)\right];$
$\rho < -\rho^*$ and $\rho' > -\rho^*$,	$\frac{1}{2\pi(1+\kappa^{\frac{1}{2}})}\exp\left\{\frac{-[\rho-\kappa^{\frac{1}{2}}\rho'+(1-\kappa^{\frac{1}{2}})\rho^*]^2}{4\kappa\pi}\right\}\left[1+\phi\left(\frac{\rho+\kappa^{\frac{1}{2}}\rho'+(1-\kappa^{\frac{1}{2}})\rho^*}{2(\kappa\pi)^{\frac{1}{2}}}\right)\right]$ $+\frac{1-\kappa^{\frac{1}{2}}}{2\pi(1+\kappa^{\frac{1}{2}})^2}\exp\left\{\frac{-[\rho+\kappa^{\frac{1}{2}}\rho'+(1+\kappa^{\frac{1}{2}})\rho^*]^2}{4\kappa\pi}\right\}\left[1-\phi\left(\frac{\kappa^{\frac{1}{2}}\rho'-\rho-(1-3\kappa^{\frac{1}{2}})\rho^*}{2(\kappa\pi)^{\frac{1}{2}}}\right)\right];$
$\rho < -\rho^*$ and $\rho' < -\rho^*$,	$\frac{1}{\pi(1+\kappa^{\frac{1}{2}})^2}\exp\left[\frac{-(\rho-\rho')^2}{4\kappa\pi}\right]\left[1+\phi\left(\frac{\rho+\rho'+2(1-\kappa^{\frac{1}{2}})\rho^*}{2(\kappa\pi)^{\frac{1}{2}}}\right)\right].$

TABLE 5. Integral $(0,\infty)$ of a product of Green functions

$$I_3(\rho,\rho') - I_2(\rho,\rho')$$

$\rho > -\rho^*$ and $\rho' > -\rho^*$,	$\frac{1}{2\pi}\exp\left[\frac{-(\rho-\rho')^2}{4\pi}\right]\left\{\left(\frac{1-\kappa^{\frac{1}{2}}}{1+\kappa^{\frac{1}{2}}}\right)^2\left[1-\phi\left(\frac{\rho+\rho'+4\rho^*}{2\pi^{\frac{1}{2}}}\right)\right]+\phi\left(\frac{\rho+\rho'}{2\pi^{\frac{1}{2}}}\right)\right\}$ $+\frac{1-\kappa^{\frac{1}{2}}}{2\pi(1+\kappa^{\frac{1}{2}})}\exp\left[\frac{-(\rho+\rho'+2\rho^*)^2}{4\pi}\right]\left[1-\phi\left(\frac{\rho-\rho'+2\rho^*}{2\pi^{\frac{1}{2}}}\right)-\phi\left(\frac{\rho'-\rho+2\rho^*}{2\pi^{\frac{1}{2}}}\right)\right];$
$\rho > -\rho^*$ and $\rho' < -\rho^*$,	$\frac{1}{\pi(1+\kappa^{\frac{1}{2}})}\exp\left\{\frac{-[\rho'-\kappa^{\frac{1}{2}}\rho+(1-\kappa^{\frac{1}{2}})\rho^*]^2}{4\kappa\pi}\right\}\phi\left(\frac{\rho'+\kappa^{\frac{1}{2}}\rho+(1-\kappa^{\frac{1}{2}})\rho^*}{2(\kappa\pi)^{\frac{1}{2}}}\right)$ $+\frac{1-\kappa^{\frac{1}{2}}}{\pi(1+\kappa^{\frac{1}{2}})^2}\exp\left\{\frac{-[\rho'+\kappa^{\frac{1}{2}}\rho+(1+\kappa^{\frac{1}{2}})\rho^*]^2}{4\kappa\pi}\right\}\left[1-\phi\left(\frac{\kappa^{\frac{1}{2}}\rho-\rho'-(1-3\kappa^{\frac{1}{2}})\rho^*}{2(\kappa\pi)^{\frac{1}{2}}}\right)\right];$
$\rho < -\rho^*$ and $\rho' > -\rho^*$,	$\frac{1}{\pi(1+\kappa^{\frac{1}{2}})}\exp\left\{\frac{-[\rho-\kappa^{\frac{1}{2}}\rho'+(1-\kappa^{\frac{1}{2}})\rho^*]^2}{4\kappa\pi}\right\}\phi\left(\frac{\rho+\kappa^{\frac{1}{2}}\rho'+(1-\kappa^{\frac{1}{2}})\rho^*}{2(\kappa\pi)^{\frac{1}{2}}}\right)$ $+\frac{1-\kappa^{\frac{1}{2}}}{\pi(1+\kappa^{\frac{1}{2}})^2}\exp\left\{\frac{-[\rho+\kappa^{\frac{1}{2}}\rho'+(1+\kappa^{\frac{1}{2}})\rho^*]^2}{4\kappa\pi}\right\}\left[1-\phi\left(\frac{\kappa^{\frac{1}{2}}\rho'-\rho-(1-3\kappa^{\frac{1}{2}})\rho^*}{2(\kappa\pi)^{\frac{1}{2}}}\right)\right];$
$\rho < -\rho^*$ and $\rho' < -\rho^*$,	$\frac{1}{\pi(1+\kappa^{\frac{1}{2}})^2}\exp\left[\frac{-(\rho-\rho')^2}{4\kappa\pi}\right]\left[2\phi\left(\frac{\rho+\rho'+2(1-\kappa^{\frac{1}{2}})\rho^*}{2(\kappa\pi)^{\frac{1}{2}}}\right)-\frac{(1-\kappa^{\frac{1}{2}})^2}{2\kappa^{\frac{1}{2}}}\right]$ $+\frac{1-\kappa^{\frac{1}{2}}}{2\pi\kappa^{\frac{1}{2}}(1+\kappa^{\frac{1}{2}})}\exp\left[\frac{-(\rho+\rho'+2\rho^*)^2}{4\kappa\pi}\right].$

TABLE 6. Kernel of the integral equation (8.22)

REFERENCES

ABRAMOWITZ, M. & STEGUN, I. A. 1971 *Handbook of Mathematical Functions*. Dover.

ACRIVOS, A. 1971 Heat transfer at high Péclet number from a small sphere freely rotating in a simple shear field. *J. Fluid Mech.* **46**, 233–240.

ARIS, R. 1956 On the dispersion of a solute in a fluid flowing through a tube. *Proc. R. Soc. Lond.* A **235**, 67–77.

ARIS, R. 1962 *Vectors, Tensors and the Basic Equations of Fluid Mechanics*. Prentice-Hall.

BATCHELOR, G. K. 1967 *An Introduction to Fluid Dynamics*. Cambridge University Press.

BRENNER, H. 1970 Rheology of a dilute suspension of dipolar spherical particles in an external field. *J. Colloid Interface Sci.* **32**, 141–158.

BRENNER, H. 1972 Suspension rheology in the presence of rotary Brownian motion and external couples: elongational flow of dilute suspensions. *Chem. Engng Sci.* **27**, 1069–1107.

BRENNER, H. 1980*a* A general theory of Taylor dispersion phenomena. *PhysicoChem. Hydrodyn.* **1**, 91–123.

BRENNER, H. 1980*b* Dispersion resulting from flow through spatially periodic porous media. *Phil. Trans. R. Soc. Lond.* A **297**, 81–133.

BRENNER, H. 1982 A general theory of Taylor dispersion phenomena II. An extension. *PhysicoChem. Hydrodyn.* **3**, 139–157.

BRENNER, H. 1984 Antisymmetric stresses induced by the rigid-body rotation of dipolar suspensions: vortex flows. *Intl J. Engng Sci.* **22**, 645–682.

BRENNER, H. & ADLER, P. M. 1982 Dispersion resulting from flow through spatially periodic porous media II. Surface and intraparticle transport. *Phil. Trans. R. Soc. Lond.* A **307**, 149–200.

BRENNER, H. & CONDIFF, D. W. 1974 Transport mechanics in systems of orientable particles IV. Convective transport. *J. Colloid Interface Sci.* **47**, 199–264.

BRENNER, H. & WEISSMAN, M. H. 1972 Rheology of a dilute suspension of dipolar spherical particles in an external field. II. Effects of rotary Brownian motion. *J. Colloid Interface Sci.* **41**, 499–531.

CONDIFF, D. W. & DAHLER, J. S. 1964 Fluid mechanical aspects of antisymmetric stress. *Phys. Fluids* **7**, 842–854.

COX, R. G., ZIA, I. Y. Z. & MASON, S. G. 1968 Particle motions in sheared suspensions XXV. Streamlines around cylinders and spheres. *J. Colloid Interface Sci.* **27**, 7–18.

DAHLER, J. S. & SCRIVEN, L. E. 1961 Angular momentum of continua. *Nature* **192**, 36–37.

DAHLER, J. S. & SCRIVEN, L. E. 1963 Theory of structured continua I. General consideration of angular momentum and polarization. *Proc. R. Soc. Lond.* A **275**, 504–527.

ERINGEN, A. C. 1964 Simple microfluids. *Intl J. Engng Sci.* **2**, 205–217.

ERINGEN, A. C. 1966 Theory of micropolar fluids. *J. Math. Mech.* **16**, 1–18.

FRANKEL, N. A. & ACRIVOS, A. 1968 Heat and mass transfer from small spheres and cylinders freely suspended in shear flow. *Phys. Fluids* **11**, 1913–1918.

JANSONS, K. M. 1983 Determination of the constitutive equations for a magnetic fluid. *J. Fluid Mech.* **137**, 187–216.

NADIM, A. 1983 Master's dissertation, Department of Chemical Engineering, Massachusetts Institute of Technology, Cambridge, Massachusetts.

RHINES, P. B. & YOUNG, W. R. 1983 How rapidly is a passive scalar mixed within closed streamlines? *J. Fluid Mech.* **133**, 133–145.

TAYLOR, G. I. 1953 Dispersion of soluble matter in solvent flowing slowly through a tube. *Proc. R. Soc. Lond.* A **219**, 186–203.

TORZA, S., HENRY, C. P., COX, R. G. & MASON, S. G. 1971 Particle motions in sheared suspensions. XXVI. Streamlines in and around liquid drops. *J. Colloid Interface Sci.* **35**, 529–543.

TRUESDELL, C. & TOUPIN, R. 1960 The classical field theories. In *Handbuch der Physik*: Vol. III/1 (ed. S. Flügge), pp. 226–793 (see esp. p. 702). Springer-Verlag.

ZUZOVSKY, M., ADLER, P. M. & BRENNER, H. 1983 Spatially periodic suspensions of convex particles in linear shear flows III. Dilute arrays of spheres suspended in Newtonian fluids. *Phys. Fluids* **26**, 1714–1723.